THESIS FOR THE DEGREE OF LICENTIATE OF TECHNOLOGY

Microscopic modelling of exciton-exciton interactions in atomically thin semiconductors

Daniel Erkensten

Department of Physics

Chalmers University of Technology

Göteborg, Sweden 2022

Microscopic modelling of exciton-exciton interactions in atomically thin semiconductors

Daniel Erkensten

Department of Physics
Chalmers University of Technology
SE-412 96 Göteborg
Sweden
Telephone + 46 (0)31-772 1000

Cover illustration: Schematic picture of exciton-exciton interactions between interlayer excitons in a transition-metal dichalcogenide heterobilayer. Interlayer excitons exhibit a large out-of-plane dipole moment due to the spatial separation of electrons and holes and can be viewed as repelling dipoles.

Printed at Chalmers digitaltryck
Göteborg, Sweden 2022

Microscopic modelling of exciton-exciton interactions in atomically thin semiconductors

Daniel Erkensten
Department of Physics
Chalmers University of Technology

Abstract

The successful isolation and characterization of the technologically promising material graphene in 2004 has spurred huge interest in other two-dimensional materials. Transition-metal dichalcogenides (TMDs), being one such class of materials, display intriguing properties from both a fundamental and technological point of view. In particular, they constitute a platform for studying novel physical phenomena such as many-body correlations and exotic states of matter. The exceptionally strong Coulomb interaction in these materials gives rise to tightly bound excitons, i.e., electron-hole pairs, which are neither of purely fermionic nor purely bosonic character. In the weak excitation regime, it is sufficient to treat excitons as pure bosons, but as the density of excitons increases their fermionic substructure becomes important, resulting in highly non-trivial scattering characteristics between excitons.
In this work we have developed a microscopic theory of exciton-exciton interactions in TMD monolayers and van der Waals heterostructures. The latter are formed when stacking two monolayers on top of each other and this extends the rich exciton landscape to include also spatially separated interlayer excitons, consisting of electrons and holes located in different layers. We find that intralayer and interlayer excitons interact in fundamentally different ways – while intralayer excitons interact primarily through quantum-mechanical exchange interactions, interlayer excitons can be viewed as repelling dipoles. We demonstrate the crucial role of these strong repulsive dipole-dipole interactions for exciton transport and diffusion. Moreover, we shed light on the particular importance of dark excitons in the context of exciton-exciton annihilation, which crucially governs the efficiency of TMD-based optoelectronic applications. The microscopic insights gained in this work can be used to study more exotic quantum phenomena such as strong correlations or exciton-exciton interactions between hybridised exciton states in moiré materials.

Keywords: transition-metal dichalcogenides, density matrix formalism, dark excitons, exciton-exciton interactions

List of publications

This thesis contains an introductory text based on the following papers:

I. **Exciton-exciton interaction in transition metal dichalcogenide monolayers and van der Waals heterostructures**
D. Erkensten, S. Brem, E. Malic
Phys. Rev. B. **103**, 045426 (2021)

II. **Dark exciton-exciton annihilation in monolayer WSe_2**
D. Erkensten, S. Brem, K. Wagner, R. Perea-Causin, R. Gillen, J.D. Ziegler, J. Maultzsch, A. Chernikov, E. Malic
Phys. Rev. B **104**, L241406 (2021) (Editor's Suggestion)

III. **Microscopic view on repulsive dipole-dipole interaction driving interlayer exciton diffusion in van der Waals heterostructures**
D. Erkensten, S. Brem, R. Perea-Causin, E. Malic
in manuscript (submission shortly)

My contributions to the appended papers
As first-author, I developed the microscopic theory, performed the numerical calculations, analyzed the results and wrote the papers with input from my main supervisor.

Publications not appended or discussed in thesis

IV. **Topology of critical chiral phases: Multiband insulators and superconductors**
O. Balabanov, D. Erkensten, H. Johannesson
Phys. Rev. Research **3**, 043048 (2021)

V. **Fermi-Pressure and Coulomb repulsion driven rapid hot plasma expansion in a van der Waals heterostructure**
J. Choi, J. Embley, D. Blach, R. Perea-Causin, D. Erkensten, S. Brem, D. Kim, L. Yuan, T. Taniguchi, K. Watanabe, K. Ueno, E. Tutuc, E. Malic, X. Li, and L. Huang
manuscript in preparation

My contributions to the non-appended publications
In Paper IV, I set up the underlying theoretical framework and contributed in discussions. In Paper V, I took part in developing the theoretical model.

Acknowledgements

Here, I would like to single out the people who contributed directly and indirectly to the results found in this thesis. First, and above all, I want to thank my supervisor Ermin Malic. Thank you for constantly being available even though we lately have been spatially separated. Your expertise, feedback and motivation is inspiring and has helped me develop tremendously as a researcher. Secondly, I thank Samuel Brem. I am truly grateful for your constant support during the early stages of my PhD. Besides contributing with many microscopic insights in my work, you have helped me gain my independence and my confidence. Thirdly, I must thank Raul Perea-Causin for always (too often!) having your door open for discussions and brainstorming sessions. I also want to thank past and present members of the UQD group at Chalmers for creating such a welcoming and friendly work environment and my examiner, Jari Kinaret, for the detailed feedback on my thesis. The remainder of my gratitude goes to friends in and outside Academia and finally, my family. Tack!

CONTENTS

CHAPTER 1

INTRODUCTION

The isolation and characterization of the two-dimensional and purely carbon-based material graphene by Andre Geim and Konstantin Novoselov in 2004, paved the way for investigating other exotic and technologically relevant 2D materials [1]. In particular, transition-metal dichalcogenides (TMDs) has proven to be a promising class of such materials, and offer since 2010[1] a platform for studying intriguing many-body correlations and quantum phenomena at the nanoscale [3–6]. In contrast to graphene, the crystal lattice of TMDs consists of two different types of atoms and has the material composition MX_2, where the transition-metal (M=Mo, W, etc.) is sandwiched between two layers of chalcogenides (X_2=Se_2, S_2, Te_2) as shown in Fig. 1.1.

The reduced dimensionality of these materials allows for a remarkably strong Coulomb interaction between carriers leading to the formation of *excitons*, strongly bound electron-hole pairs. Excitons are dominating the optical response of TMDs and govern the efficiency of optoelectronic applications such as photodetectors or solar cells [8], and therefore a microscopic understanding

[1]This year, for the first time in history, Tony Heinz and his collaborators successfully managed to exfoliate the TMD monolayer, MoS_2, a direct-gap semiconductor [2]. The very same year, Geim and Novoselov were awarded the Nobel Prize for their groundbreaking experiments on graphene.

of these quasiparticles and their interaction mechanisms is highly desirable. In recent years, a lot of effort has been put into investigating how exciton relaxation dynamics, transport and optics is influenced by interactions between excitons and phonons [9–12], free or microcavity photons [13–15]. Here, we will instead consider interactions between excitons themselves which are commonly seen to be highly important at elevated densities of electrons and holes and results in a number of intriguing purely quantum phenomena such as excitation-induced dephasing [16, 17], exciton-exciton annihilation [18, 19], density-dependent energy renormalizations [20–22] and non-linear exciton transport [23–25].

Treating exciton-exciton interactions on a microscopic footing poses a challenging problem as, although excitons can be treated as non-interacting neutral bosons in the low excitation regime, their fermionic substructure has to be incorporated in the scattering characteristics at higher densities [26].

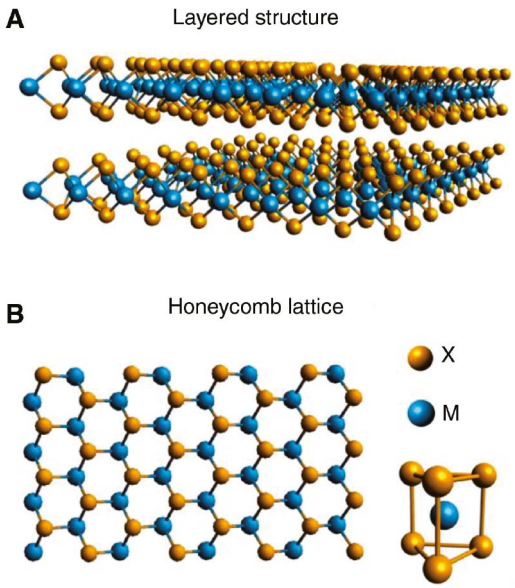

Figure 1.1: TMD monolayers from the side (A) and from the top (B), revealing its honeycomb crystal structure. Figure adapted from [7].

Moreover, the rich exciton landscape of TMDs consisting of bright[2] (intravalley) and dark[3] (intervalley) exciton states [31, 32] (cf. Fig. 1.2(a)) enables a large number of available interaction mechanisms. By stacking two (or more) TMD layers on top of each other, resulting in a van der Waals heterostructure or heterobilayer [33], the exciton landscape becomes even richer, now including also interlayer excitons, consisting of electrons and holes in different layers as shown in Fig. 1.2(b). Due to the spatial separation of electrons and holes, interlayer excitons are long-lived and exhibit permanent out-of-plane dipole moments, which potentially makes them useful in the realization of electrically controlled devices [34–36]. Moreover, the dipolar and repulsive nature of these excitons prevents the formation of exciton complexes such as biexcitons, facilitating exciton condensation [3, 4].

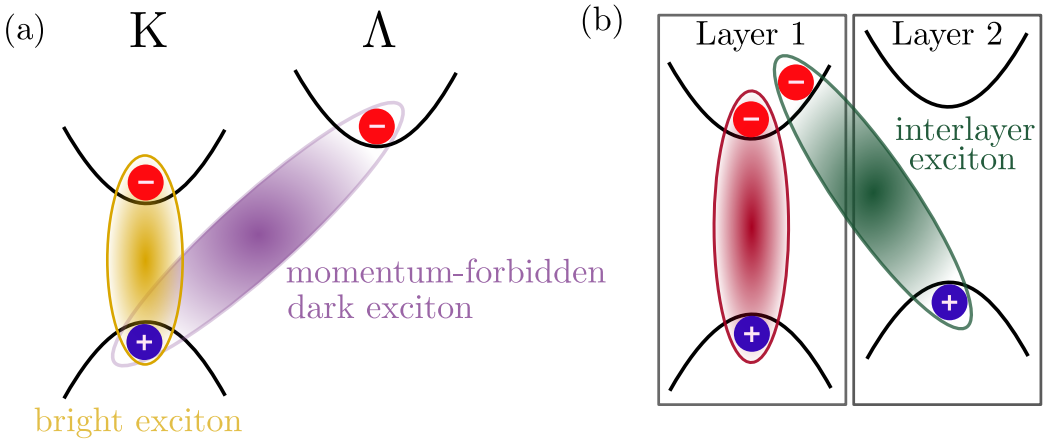

Figure 1.2: Different types of exciton species in TMD monolayers and van der Waals heterostructures. (a) Bright KK excitons (yellow) and dark KΛ excitons (purple) in an exemplary TMD monolayer. (b) Intra- (red) and interlayer (green) excitons in an exemplary TMD bilayer.

[2]The wording "bright" refers to the fact that intravalley excitons can be accessed via light and optical excitation. In contrast, dark excitons have finite center-of-mass momenta [27], which can not be accessed by light but have to be provided via e.g. scattering with phonons [12, 28, 29].

[3]In this thesis, the terminology "dark excitons" and "intervalley excitons" is used interchangeably. However, note that the former may also refer to so-called spin-dark excitons, where the electrons and holes forming the excitons have opposite spins [30].

In this thesis, we investigate exciton-exciton interactions in monolayer transition-metal dichalcogenides and heterobilayers on a microscopic footing and unveil the mechanisms behind exciton-exciton scattering, exciton-exciton annihilation and non-linear exciton propagation. In particular, we find that different types of excitons interact in fundamentally different ways: intralayer excitons display strong quantum-mechanical exchange interactions due to their fermionic substructure, and interlayer excitons interact mainly through strong repulsive dipole-dipole interactions. The obtained microscopic insights can potentially be used to optimize the efficiency of future TMD-based devices and the established theoretical framework could be extended also to more exotic systems such as moiré materials[4].

1.1 Outline

We start out this thesis by providing an introduction to the theoretical framework used to model two-dimensional semiconductors, i.e the second quantization formalism and the Heisenberg picture. In particular, we show how the relevant interaction mechanisms between charge carriers can be reformulated in terms of excitonic quantities and interactions. In Chapter 3, which is based on Papers I and III, we present the general theory of exciton-exciton interactions and reveal the leading interaction mechanisms in TMD monolayers and heterostructures. The general framework laid out in Chapter 3, sets the stage for investigating the impact of exciton-exciton interactions on non-linear exciton propagation in Chapter 4. In Chapter 5, we discuss a completely different type of exciton-exciton interaction process than the one considered in Chapters 3 and 4, referred to as exciton-exciton annihilation, summarizing Paper II. Finally, we provide some concluding remarks and a future outlook in Chapter 6.

[4]A boom in moiré physics research, i.e. the study of materials which exhibit a moiré pattern such as twisted heterostructures or multilayers [37], followed after the discovery of the superconducting properties in twisted bilayer graphene by Herrero and collaborators in 2018 [38].

CHAPTER 2

THEORETICAL FRAMEWORK

In this chapter we will give a brief introduction to the theoretical framework used to model many-body phenomena in two-dimensional semiconductors. The theoretical approach relies heavily on the concept of second quantization, also known as canonical quantization, a formalism commonly used to describe many-body quantum systems. Here, we will not give any derivation of the formalism (as this can be found in various text books on quantum field theory, see e.g. [39, 40]) but only provide the necessary interaction mechanisms of relevance to this work and the appended papers.

In quantum mechanics, we usually distinguish between two different types of particles: *bosons* and *fermions*.[1] The former can in second quantization formalism be represented by *commuting* creation operators $b_i^\dagger$ (or annihilation operators b_i) and the latter are represented by *anti-commuting* operators $a_i^{(\dagger)}$ such that

$$\begin{aligned} \{a_i, a_j^\dagger\} &= \delta_{i,j} \quad \text{(fermions)} \\ [b_i, b_j^\dagger] &= \delta_{i,j} \quad \text{(bosons)} \end{aligned} \tag{2.1}$$

[1] There are exceptions to this rule which are referred to as *anyons*. These exotic quasi-particles only appear in two-dimensional quantum systems and do not just pick up a plus-sign or a minus-sign when exchanged but an imaginary phase-factor $e^{i\theta}$, $\theta \in [0,\pi]$ [41].

Note that the operators are decorated with the compound indices i, j. These indices provide information about the state of the particles, such as their momentum, spin, and in which band and valley[2] they reside in. Typical examples of bosons are phonons or photons and common fermions are electrons or holes (signifying a vacancy in the valence band, i.e. the absence of an electron). Depending on the density, also excitons although formally being a combination of electrons and holes, can be described as non-interacting bosons [42–44]. This will be further discussed in the following chapters. For now, we will only be considering interactions between purely fermionic particles. The interactions are summarized in a single many-particle Hamiltonian, H, whose individual contributions will be discussed in detail below.

2.1 Many-particle Hamilton operator

The many-particle Hamilton operator H of relevance in this work can be written as $H = H_0 + H_{\mathrm{c-c}}$, where H_0 is the non-interacting kinetic contribution and $H_{\mathrm{c-c}}$ is the carrier-carrier interaction.[3] The former reads

$$H_0 = \sum_{\mathbf{l}} \epsilon_{\mathbf{l}} a_{\mathbf{l}}^\dagger a_{\mathbf{l}} \ , \tag{2.2}$$

with the electronic band structure $\epsilon_{\mathbf{l}}$. Here, the compound index $\mathbf{l}$ includes momentum $\mathbf{k}_l$, band λ_l and spin σ_l.[4] In the case of materials which exhibit a parabolic band structure around the high-symmetry points in the Brillouin zone such as transition-metal dichalcogenides [45], we can make use of the *effective mass approximation* [46] to write

$$\epsilon_{\boldsymbol{k}}^{\lambda} = \epsilon_0^{\lambda} + \sigma_{\lambda} \frac{\hbar^2 \boldsymbol{k}^2}{2m^{\lambda}} \ , \tag{2.3}$$

[2] We will make use of the word valley in the context of intra- and intervalley excitons extensively in this thesis. The electronic band structure of transition-metal dichalcogenides exhibits multiple valleys in the first Brillouin zone, that is, local extrema, in which it is energetically favorable for a particle to reside in.

[3] As we are exclusively interested in exciton-exciton interactions in this work we do not include contributions from phonons or photons and their interactions with electrons here.

[4] The spin index σ will not be of relevance in this work and is only included for completeness here.

where, $\sigma_\lambda = +1$ (-1) for $\lambda = c$ $(\lambda = v)$, c being a conduction band and v being a valence band. The momentum $\boldsymbol{k}$ is expressed relative to the considered high-symmetry point in the Brillouin zone and m^λ is the effective mass in band λ. The effective mass is directly related to the (inverse) curvature of the band such that $1/m^\lambda = \frac{\partial^2 \epsilon^\lambda_{\boldsymbol{k}}}{\partial^2 \boldsymbol{k}}/\hbar^2$, and is commonly directly extracted from the single-particle band structure, which in turn is obtained from *ab-initio* calculations. Here, we define both electron and hole masses positive such that $m_v \equiv m_h > 0$.

The interaction between charge carriers is of fundamental importance in this work. It can be represented by the following general two-particle interaction:

$$H_{\mathrm{c-c}} = \frac{1}{2} \sum_{\mathbf{i,j,k,l}} V^{\mathbf{ijkl}} a^\dagger_{\mathbf{i}} a^\dagger_{\mathbf{j}} a_{\mathbf{k}} a_{\mathbf{l}} \ , \tag{2.4}$$

where $V^{\mathbf{ijkl}}$ is the *Coulomb matrix element* defined by

$$V^{\mathbf{ijkl}} = \sum_{\boldsymbol{q}} V_{\boldsymbol{q}}^{\lambda_i \lambda_j \lambda_k \lambda_l} F_{il}(\boldsymbol{q}) F_{jk}(-\boldsymbol{q}) \ , F_{fi}(\boldsymbol{q}) = \langle f | \mathrm{e}^{i\boldsymbol{q}\cdot\boldsymbol{r}} | i \rangle \ , \tag{2.5}$$

where the form-factor $F_{fi}(\boldsymbol{q})$ describes the probability of scattering from an initial state i to a final state f with the momentum transfer $\boldsymbol{q}$. The Coulomb interaction $V_{\boldsymbol{q}}^{\lambda_i \lambda_j \lambda_k \lambda_l}$ includes intraband ($\lambda_i = \lambda_l$, $\lambda_j = \lambda_k$) as well as interband ($\lambda_i \neq \lambda_l$, $\lambda_j \neq \lambda_k$) transitions. To develop a material-specific model we also include a Keldysh-like dielectric screening function [47–50] to take finite thickness effects as well as screening from surrounding substrates into account when evaluating the Coulomb interaction potential $V_{\boldsymbol{q}}^{\lambda_i \lambda_j \lambda_k \lambda_l}$, discussed in detail below. For scattering processes with *small* momentum transfer $\boldsymbol{q}$ (compared to the Brillouin zone) we may approximate the form-factors as follows:

$$F_{fi}(\boldsymbol{q}) = \langle \boldsymbol{k}_f, \lambda_f | \mathrm{e}^{i\boldsymbol{q}\cdot\boldsymbol{r}} | \boldsymbol{k}_i, \lambda_i \rangle \approx \delta_{\lambda_i, \lambda_f} \delta_{\boldsymbol{q}, \boldsymbol{k}_f - \boldsymbol{k}_i} + i\boldsymbol{q} \cdot \langle \boldsymbol{k}_f, \lambda_f | \boldsymbol{r} | \boldsymbol{k}_i, \lambda_i \rangle \ , \tag{2.6}$$

where we have approximated the initial and final states as Bloch states, i.e. $\langle \boldsymbol{r} | i \rangle = \mathrm{e}^{i\boldsymbol{k}_i \cdot \boldsymbol{r}} u_{\lambda_i \boldsymbol{k}_i}(\boldsymbol{r})$. Hence, we deduce, to leading order, that the intraband Coulomb matrix element scales with the Coulomb potential $V_{\boldsymbol{q}}$ and the interband element scales as $V_{\boldsymbol{q}} |\boldsymbol{q} \cdot \boldsymbol{M}|^2$, $|\boldsymbol{M}|^2 = |\langle \boldsymbol{k}_f, \lambda_f | \nabla_{\boldsymbol{k}} | \boldsymbol{k}_i, \lambda_i \rangle|^2 \sim |\langle \boldsymbol{k}_f, \lambda_f | \boldsymbol{r} | \boldsymbol{k}_i, \lambda_i \rangle|^2$ being the (squared) optical matrix element[5]. A similar

[5]Note that the quantity $\langle \boldsymbol{k}_f, \lambda_f | \boldsymbol{r} | \boldsymbol{k}_i, \lambda_i \rangle$ refers to the dipole matrix element, but by taking the expectation value in momentum space instead of real space and considering $i \langle \boldsymbol{k}_f, \lambda_f | \nabla_{\boldsymbol{k}} | \boldsymbol{k}_i, \lambda_i \rangle$ we retrieve the optical matrix element.

estimate of the form-factors as the one above can be made within a tight-binding framework [51, 52]. For scattering processes involving a large momentum transfer, the form-factors have to be extracted from *ab-initio* calculations. Such processes are referred to as intervalley processes, in which electrons and holes scatter from one high-symmetry point in the Brillouin zone to another, and are discussed in the context of Auger recombination processes in Chapter 5 based on Paper II.

A two-band model including one conduction band c and one valence band v ($\lambda = c,v$) constitutes an important example. In this specific case we may express the Coulomb interaction in the following fashion, separating intraband and interband contributions[6]:

$$H_{c-c} = \frac{1}{2}\sum_{\substack{\boldsymbol{k},\boldsymbol{k'},\boldsymbol{q}\\ \lambda,\bar{\lambda}}} V_{\boldsymbol{q}}^{\lambda\bar{\lambda}\bar{\lambda}\lambda}\lambda^{\dagger}_{\boldsymbol{k}+\boldsymbol{q}}\bar{\lambda}^{\dagger}_{\boldsymbol{k'}-\boldsymbol{q}}\bar{\lambda}_{\boldsymbol{k'}}\lambda_{\boldsymbol{k}} + \frac{1}{2}\sum_{\substack{\boldsymbol{k},\boldsymbol{k'},\boldsymbol{q}\\ \lambda\neq\bar{\lambda}}} V_{\boldsymbol{q}}^{\lambda\bar{\lambda}\lambda\bar{\lambda}}\lambda^{\dagger}_{\boldsymbol{k}+\boldsymbol{q}}\bar{\lambda}^{\dagger}_{\boldsymbol{k'}-\boldsymbol{q}}\lambda_{\boldsymbol{k'}}\bar{\lambda}_{\boldsymbol{k}} \ . \quad (2.7)$$

Here, we have excluded terms with an odd number of conduction band or valence band electrons, i.e. processes associated with Auger recombination or impact excitation [53, 54]. This type of processes is discussed in detail in Chapter 5. Furthermore, note that we focus on the long-range part of the interaction and thereby set the Coulomb matrix elements to

$$V_{\boldsymbol{q}}^{\lambda\bar{\lambda}\bar{\lambda}\lambda} \approx V_{\boldsymbol{q}} \ \ \text{(intraband)} \ , \quad (2.8)$$

and

$$V_{\boldsymbol{q}}^{\lambda\bar{\lambda}\lambda\bar{\lambda}} \approx V_{\boldsymbol{q}}|\boldsymbol{q}\cdot\boldsymbol{M}^{\lambda\bar{\lambda}}|^2 \ \ \text{(interband)} \ , \quad (2.9)$$

following our approximations above. In this work, we consider the *screened* two-dimensional Coulomb potential

$$V_{\boldsymbol{q}} = \frac{V_{\text{bare},\boldsymbol{q}}}{\varepsilon_{\boldsymbol{q}}} \ , V_{\text{bare},\boldsymbol{q}} = \frac{e^2}{2\epsilon_0 A|\boldsymbol{q}|} \ , \quad (2.10)$$

where A is the crystal area, e is the electric charge, ϵ_0 is the vacuum permittivity and $\varepsilon_{\boldsymbol{q}}$ is the dielectric screening. For TMD monolayers[7] the screening

[6] Note, in particular, the ordering of indices in the Coulomb matrix element and the simplified notation of the fermionic operators compared to (2.4), taking $a^{(\dagger)}_{\lambda\boldsymbol{k}} \to \lambda^{(\dagger)}_{\boldsymbol{k}}$.

[7] In Papers I and III we also considered TMD monolayers stacked on top of each other forming van der Waals heterostructures. In this case the Keldysh screening has to be generalized, which can be done by solving the Poisson equation for a multilayer system [35, 55].

is described within a Rytova-Keldysh framework [47, 48] given by the dielectric function [12]:

$$\varepsilon_{\boldsymbol{q}} = \kappa_{\mathrm{TMD}} \tanh[\frac{1}{2}(\alpha_{\mathrm{TMD}} dq - \ln(\frac{\kappa_{\mathrm{TMD}} - \kappa_{\mathrm{sub}}}{\kappa_{\mathrm{TMD}} + \kappa_{\mathrm{sub}}}))] \ , \tag{2.11}$$

where d is the layer thickness of the TMD, $\kappa_{\mathrm{TMD}} = \sqrt{\varepsilon^{||}\varepsilon^{\perp}}$, $\alpha_{\mathrm{TMD}} = \sqrt{\frac{\varepsilon^{||}}{\varepsilon^{\perp}}}$, $\varepsilon^{||}$ and $\varepsilon^{\perp}$ being the in-plane and out-of-plane components of the dielectric tensor of the TMD respectively and κ_{sub} is the effective dielectric constant of the surrounding substrate, here assumed to be given by the average of the dielectric constants above and below the TMD. The material-specific dielectric constants are extracted from ab-initio calculations [56, 57]. A linearized version of (2.11) is commonly used which holds assuming $dq << 1$ and $\kappa_{\mathrm{sub}} << \kappa_{\mathrm{TMD}}$:

$$\varepsilon_{\boldsymbol{q}} = \kappa_{\mathrm{sub}} + \frac{d\varepsilon^{||} q}{2} \ . \tag{2.12}$$

When describing scattering processes involving a large momentum transfer one has to extract the screening from *ab-initio* calculations or consider a more refined screening model than the one provided by (2.11).[8]

2.2 Heisenberg's equation of motion

Having microscopic access to all relevant interaction mechanisms through the Hamiltonian, H, we can now use H to investigate how certain observables evolve in time by exploiting a Heisenberg's equation of motion approach. In the Heisenberg picture, observables are described as expectation values of time-dependent operators and their time evolution is governed by the following equation of motion:

$$i\hbar \frac{d}{dt}\langle A \rangle = \langle [A, H] \rangle \ , \tag{2.13}$$

[8] In Paper II, we considered exciton scattering processes which involves a large momentum transfer on the order of the reciprocal lattice vector, and therefore we adapted an analytic screening model [50] which is in good agreement with ab-initio calculations [58, 59] also in the short wave-length limit.

where A is the operator of interest, here assumed to be *explicitly* time-independent. Note that the operator A in principle can consist of any combination of bosonic and fermionic creation and annihilation operators. Here, we shall be concerned with the dynamics of primarily two types of quantities[9]: microscopic polarisations $p_{\boldsymbol{k},\boldsymbol{k'}} = \langle c^\dagger_{\boldsymbol{k}} v_{\boldsymbol{k'}} \rangle$, describing a single electronic transition from a valence band to a conduction band ($p^*_{\boldsymbol{k},\boldsymbol{k'}}$ results in the opposite process) and the electron (hole) occupations $f^e_{\boldsymbol{k}} = \langle c^\dagger_{\boldsymbol{k}} c_{\boldsymbol{k}} \rangle$ ($f^v_{\boldsymbol{k}} = \langle v_{\boldsymbol{k}} v^\dagger_{\boldsymbol{k}} \rangle$). The hole occupation describes the occupation in the valence band after an optical excitation. More generally, the microscopic polarisation and the occupations are off-diagonal and diagonal elements of a density matrix respectively, and the common framework in which these quantities are dealt with is referred to as the *density matrix formalism* [60]. For now, we will only consider the equation of motion for the polarisation:

$$\begin{aligned} i\hbar \dot{p}_{\boldsymbol{k},\boldsymbol{k'}} &= (\epsilon^v_{\boldsymbol{k'}} - \epsilon^c_{\boldsymbol{k}}) p_{\boldsymbol{k},\boldsymbol{k'}} \\ &+ \sum_{\boldsymbol{k}_1,\boldsymbol{q},\lambda} (V^{v\lambda\lambda v}_{\boldsymbol{q}} \langle c^\dagger_{\boldsymbol{k}} \lambda^\dagger_{\boldsymbol{k}_1-\boldsymbol{q}} \lambda_{\boldsymbol{k}_1} v_{\boldsymbol{k'}-\boldsymbol{q}} \rangle + V^{\lambda cc\lambda}_{\boldsymbol{q}} \langle \lambda^\dagger_{\boldsymbol{k}_1+\boldsymbol{q}} c^\dagger_{\boldsymbol{k}-\boldsymbol{q}} \lambda_{\boldsymbol{k}_1} v_{\boldsymbol{k'}} \rangle) \ , \end{aligned} \tag{2.14}$$

where we neglected the interband contributions. Now, we have encountered a typical problem when dealing with equations of motion and many-particle interactions: the single-particle quantity ($\propto \langle a^\dagger_i a_j \rangle$) in the left-hand side of the equation couples to a two-particle quantity ($\propto \langle a^\dagger_i a^\dagger_j a_k a_l \rangle$), which in turn needs to be evaluated, leading to a system of differential equations which is not closed. This is referred to as the *hierarchy problem* and is commonly solved by applying a correlation expansion and systematic truncation. In general, any N-operator quantity can be factorized into correlations denoted by $\langle ... \rangle^c$ of lower order [60]. Here, we will just provide the important cluster expansion for a fermionic two-particle expectation value, the so-called Hartree-Fock factorization:[10]

$$\langle a^\dagger_i a^\dagger_j a_k a_l \rangle = \langle a^\dagger_j a_k \rangle \langle a^\dagger_i a_l \rangle - \langle a^\dagger_j a_l \rangle \langle a^\dagger_i a_k \rangle + \langle a^\dagger_i a^\dagger_j a_k a_l \rangle^c \ . \tag{2.15}$$

Now, one may treat the theory on a *Hartree-Fock level* or a mean-field level, which simplifies the system to a single-particle problem in which the many-

[9] In the following chapters we will also be concerned with occupations of excitons, described by the expectation value $\langle c^\dagger_{\boldsymbol{k}} v_{\boldsymbol{k'}} v^\dagger_{\boldsymbol{k'}} c_{\boldsymbol{k}} \rangle$. However, we will express this quantity in terms of excitonic operators for simplicity, see Section 2.3.

[10] A similar expansion can be made for bosonic operators, $b^{(\dagger)}_i$, but then the intermediate minus sign becomes a plus sign, reflecting their commuting nature.

body correlations ($\langle ... \rangle^c$) are dropped. However, in order to describe scattering processes such as carrier-carrier scattering or exciton-exciton scattering (briefly discussed in the following chapter and in detail in Paper I) or the formation of bound particles, the correlations have to be kept. Here, we apply the Hartree-Fock approximation (2.15) to Eq. (2.14) and deduce

$$i\hbar \dot{p}_{\boldsymbol{k},\boldsymbol{k'}} = (\tilde{\epsilon}^v_{\boldsymbol{k'}} - \tilde{\epsilon}^c_{\boldsymbol{k}}) p_{\boldsymbol{k},\boldsymbol{k'}} - (1 - f^c_{\boldsymbol{k}} - f^v_{\boldsymbol{k}}) \sum_{\boldsymbol{q}} V^{cvvc}_{\boldsymbol{q}} p_{\boldsymbol{k}+\boldsymbol{q},\boldsymbol{k'}+\boldsymbol{q}} \ , \tag{2.16}$$

with the renormalized band energies

$$\tilde{\epsilon}^\lambda_{\boldsymbol{k}} = \epsilon^\lambda_{\boldsymbol{k}} - \sum_{\boldsymbol{q}} V^{\lambda\lambda\lambda\lambda}_{\boldsymbol{q}} f^\lambda_{\boldsymbol{k}+\boldsymbol{q}} \ . \tag{2.17}$$

In the low and intermediate excitation regime we may neglect the phase-space filling factor and set $1 - f^e_{\boldsymbol{k}} - f^v_{\boldsymbol{k}} \approx 1$, which simplifies the equations drastically. However, when treating exciton-exciton interactions which become important at high electron-hole densities, the phase-space filling factors have to be kept, as discussed in detail in Section 3.3. Let us now consider (2.16) in detail, in this chapter assuming the low excitation regime. The presence of the second term, which is due to the electron-hole interactions gives, as we shall see, rise to excitons.

2.3 The emergence of excitons

We shall now show that the electron-hole interaction results in bound excitons, quasiparticles which are Coulomb-bound electron-hole pairs and fulfill a Schrödinger-like eigenvalue problem. Assuming small densities of electrons and holes, the eigenfrequency of the polarisation is given by precisely the transition energy $\epsilon^c_{\boldsymbol{k}} - \epsilon^v_{\boldsymbol{k'}}$ (up to a factor $\hbar$), but the presence of the electron-hole Coulomb interaction leads to a mixing of different electronic states, which makes the electron momenta $\boldsymbol{k}, \boldsymbol{k'}$ bad quantum numbers. Instead, we seek a new basis which is diagonal in its quantum numbers. This can be easily achieved by transforming the electronic momenta $\boldsymbol{k}, \boldsymbol{k'}$ to center-of-mass momentum $\boldsymbol{Q}$ and relative momentum $\boldsymbol{q}$ defined according to

$$\boldsymbol{Q} = \boldsymbol{k} - \boldsymbol{k'} \ , \boldsymbol{q} = \beta \boldsymbol{k} + \alpha \boldsymbol{k'} \ , \tag{2.18}$$

introducing the mass ratios $\beta = \frac{m_e}{m_e+m_h}$ and $\alpha = \frac{m_h}{m_e+m_h}$. Secondly, note that, in the vicinity of band extrema, the electronic dispersion can be well approximated by a parabolic dispersion (Eq. (2.3)) such that:

$$\epsilon^c_{\boldsymbol{k}} - \epsilon^v_{\boldsymbol{k'}} = \frac{\hbar^2 \boldsymbol{k}^2}{2m_e} + \frac{\hbar^2 \boldsymbol{k'}^2}{2m_h} + E_g = \frac{\hbar^2 \boldsymbol{Q}^2}{2M} + \frac{\hbar^2 \boldsymbol{q}^2}{2\mu} + E_g \ , \tag{2.19}$$

where $M = m_e + m_h$ and $\mu = \frac{m_e m_h}{m_e+m_h}$ is the total and reduced mass of an electron-hole pair respectively and $E_g = \epsilon^c_0 - \epsilon^v_0$ is the quasiparticle band gap. Importantly, the center-of-mass and relative motion has been decoupled through the effective mass approximation. Hence, we may project our microscopic polarisation $p_{\boldsymbol{k},\boldsymbol{k'}}$ to an *excitonic basis* such that

$$p_{\boldsymbol{k},\boldsymbol{k'}} \to p_{\boldsymbol{q},\boldsymbol{Q}} = \sum_n \varphi^*_{n,\boldsymbol{q}} P_{n,\boldsymbol{Q}} \ , \tag{2.20}$$

defining the orthonormal[11] excitonic wave functions $\varphi_{n,\boldsymbol{q}}$, n numbering the excitonic state, and $P_{n,\boldsymbol{Q}}$ being the excitonic polarisation. With the introduced definitions above and assuming the low density limit (2.16) transforms into

$$\dot{P}_{n,\boldsymbol{Q}} = \frac{i}{\hbar}(\frac{\hbar^2 \boldsymbol{Q}^2}{2M} + E_g + E_n) P_{n,\boldsymbol{Q}} \ , \tag{2.21}$$

where the eigenenergies E_n and associated eigenfunctions are obtained from the *Wannier equation*:[12]

$$\frac{\hbar^2 \boldsymbol{q}^2}{2\mu} \varphi_{n,\boldsymbol{q}} - \sum_{\boldsymbol{k}} V^{cvvc}_{\boldsymbol{k}} \varphi_{n,\boldsymbol{k}+\boldsymbol{q}} = E_n \varphi_{n,\boldsymbol{q}} \ . \tag{2.22}$$

Now, let us admire the simplicity of the equation above. We have just obtained an equation describing Wannier[13] excitons which is in perfect analogy

[11] The excitonic wave functions fulfill both the orthogonality relation, $\sum_{\boldsymbol{k}} \varphi^*_{n,\boldsymbol{k}} \varphi_{m,\boldsymbol{k}} = \delta_{n,m}$ and the completeness relation $\sum_n \varphi^*_{n,\boldsymbol{k}} \varphi_{n,\boldsymbol{k'}} = \delta_{\boldsymbol{k},\boldsymbol{k'}}$

[12] At elevated densities of electrons and holes, the Wannier equation has to be modified to also include phase-space filling factors. Here, and in Papers I-II, we stay in an intermediate excitation regime in which we can stick to this simpler equation. In Paper III, we include the phase-space filling in the corresponding mean-field exciton-exciton interaction matrix elements, cf. Section 3.4.

[13] Formally, one distinguishes between Wannier excitons [61] which are excitons with a Bohr radius (spatial extension) larger than the lattice spacing as is typically the case in semiconductors and Frenkel excitons [62] which extend over a unit cell, typically found in molecular crystals [63]. In fact, Edward Frenkel himself was first to propose the concept of excitons in 1931.

to the corresponding time-independent Schrödinger equation for a hydrogen atom. Similarly, as the hydrogen atom, the energy levels of excitons follow a Rydberg-like series, $n = 1s,2p,2s...$, up to the continuum, as is shown in Fig. 2.1 (b). However, importantly, in contrast to free hydrogen atoms, excitons in two-dimensional semiconductors are screened by its environment, that is by the TMD itself and its surrounding substrate which crucially impacts the strength of the Coulomb interaction, through the dielectric screening $\varepsilon_{\boldsymbol{q}}$, cf. (2.11). Moreover, as already hinted about in the previous chapter, the elec-

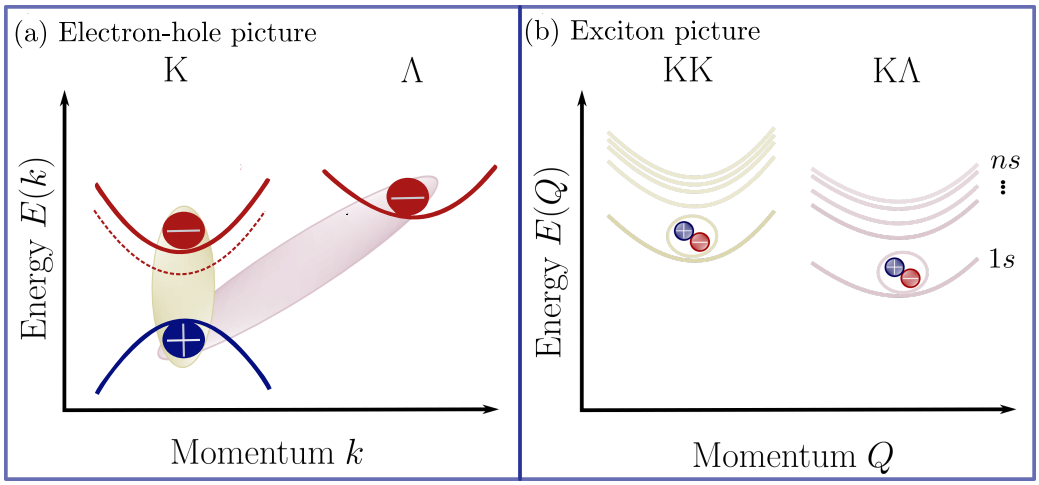

Figure 2.1: Exemplary excitons in the electron-hole picture and the excitonic picture for a W-based TMD monolayer. (a) Electrons and holes residing around the same high-symmetry point (K) form intravalley KK excitons (yellow). Electrons and holes may also form e.g. KΛ (or KK') intervalley excitons (pink). The spin polarisations of the bands are indicated by solid and dashed lines respectively, and here we only consider spin-allowed, so-called A excitons. (b) In the excitonic picture, excitons exhibit a parabolic dispersion and form a Rydberg-like series of exciton states.

trons and holes do not have to reside at the same high-symmetry point in the Brillouin zone, but can form so-called (momentum)-dark or intervalley excitons through the scattering with phonons [64, 65]. Remarkably, even though the Λ-point lies above the K-point in the electron-hole picture in tungsten-based TMDs (Fig. 2.1(a)), the excitonic dark KΛ state lies energetically below the bright state in the exciton picture (Fig. 2.1(a)), due to the large electron mass at the Λ-point.

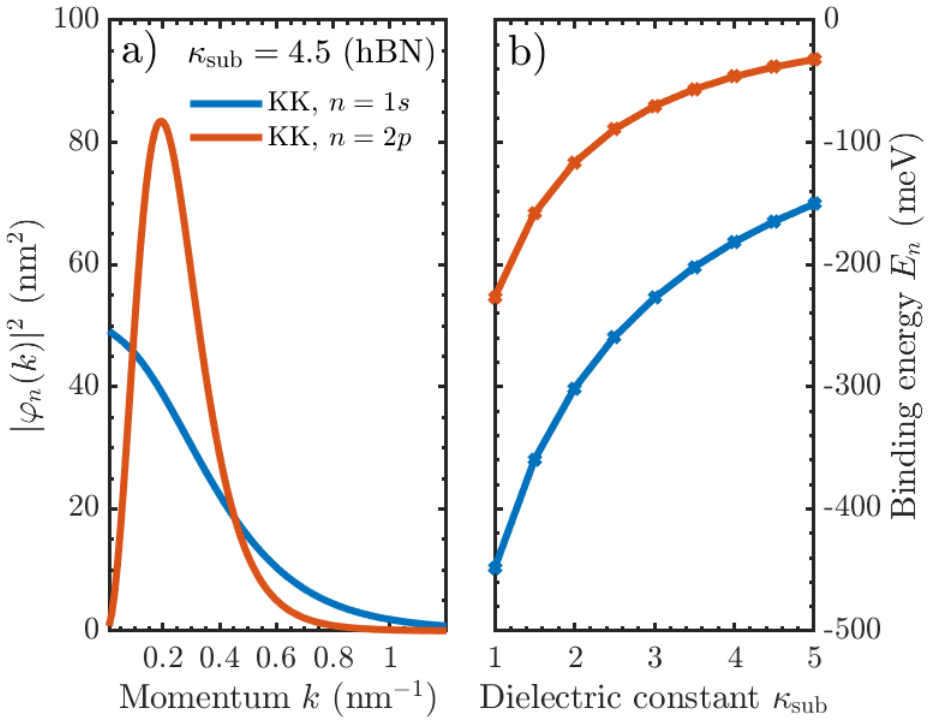

Figure 2.2: Wave functions and binding energies of KK excitons. (a): Excitonic wave functions for KK 1s and 2p excitons in hBN-encapsulated monolayer WSe_2. (b): Excitonic binding energies as a function of the dielectric constant.

By numerically solving the eigenvalue problem in (2.22) employing the screening-dependent electron-hole interaction (2.10) with material-specific parameters taken from DFT calculations, we get access to the full energy spectrum of excitons. In Fig. 2.2(a), we illustrate the 1s and 2p KK excitonic wave functions in monolayer WSe_2 encapsulated in the commonly used substrate hexagonal boron nitride (hBN), revealing the common (radial) shape of s and p-states. As shown in Fig. 2.2 (b), the excitonic binding energies in TMDs are of several hundreds of meV, and are significantly reduced when increasing the dielectric constant of the surrounding substrate. The huge binding energies found in TMDs enable excitons to be stable even at room temperature.

2.4 Developing the excitonic Hamiltonian

In the previous section we outlined a general recipe for how excitonic effects can be accounted for in a microscopic theory. Firstly, we provided the interactions of interest in the electron-hole picture and secondly, we found the equation of motion for an observable of our interest (e.g. the microscopic polarisation or electron/hole occupation) by means of Heisenberg's equation of motion and finally, we transformed the resulting equations of motion into an excitonic basis. An alternative approach relies on starting from a Hamiltonian which contains the excitonic effects from the beginning, i.e. is expressed through *excitonic operators*. This approach is highly convenient when it comes to treating interactions and scattering between excitons as it drastically reduces the number of operators needed to describe the dynamics. We will only sketch the derivation of the excitonic Hamiltonian[14] here and refer the interested reader to the works by Katsch et al. [42] (in the specific context of excitons) and Ivanov and Haug [43] for a more general treatment.

Note that we may represent the creation and annihilation of an exciton with the *pair operators*

$$P^\dagger_{\boldsymbol{k}_1,\boldsymbol{k}_2} = c^\dagger_{\boldsymbol{k}_1} v_{\boldsymbol{k}_2} \ , P_{\boldsymbol{k}_1,\boldsymbol{k}_2} = v^\dagger_{\boldsymbol{k}_2} c_{\boldsymbol{k}_1} \ , \tag{2.23}$$

respectively. Here, we choose to only assign the operators different momenta $\mathbf{k}_1, \mathbf{k}_2$ for simplicity and omit their dependence on other degrees of freedom, such as valley and spin. From the construction in (2.23), it is a simple matter to derive commutator relations for the pair operators:

$$[P_{\boldsymbol{k}_1,\boldsymbol{k}_2}, P_{\boldsymbol{k}_3,\boldsymbol{k}_4}] = [P^\dagger_{\boldsymbol{k}_1,\boldsymbol{k}_2}, P^\dagger_{\boldsymbol{k}_3,\boldsymbol{k}_4}] = 0 \ , \tag{2.24}$$

and

$$[P_{\boldsymbol{k}_1,\boldsymbol{k}_2}, P^\dagger_{\boldsymbol{k}_3,\boldsymbol{k}_4}] = \delta^{\boldsymbol{k}_1,\boldsymbol{k}_3}_{\boldsymbol{k}_2,\boldsymbol{k}_4} - \delta_{\boldsymbol{k}_2,\boldsymbol{k}_4} c^\dagger_{\boldsymbol{k}_3} c_{\boldsymbol{k}_1} - \delta_{\boldsymbol{k}_1,\boldsymbol{k}_3} v_{\boldsymbol{k}_2} v^\dagger_{\boldsymbol{k}_4} \ . \tag{2.25}$$

[14] Historically, the excitonic Hamiltonian was first introduced through the boson formalism by Usui in 1960 [44] shortly followed by works from Marumori [66] and Hanamura [67]. However, here we employ the unit operator technique introduced by Ivanov and Haug in 1993 [43] and outlined in detail in [42]. A generalization of the exciton Hamiltonian to twisted heterostructures, including so-called hybrid excitons [68] where the excitons are combinations of intra- and interlayer excitons, was recently made [69, 70].

where we made use of (2.1). Just from these two equations we can realize two fundamental insights about excitons. First, note that (2.24) states that two electron-hole pair annihilation or creation operators are symmetric under exchange. Secondly, (2.25) illustrates that excitons, in general, are *neither* bosons or fermions. In the weak excitation regime, in which the two-operator quantities $c^\dagger_{\boldsymbol{k}_3} c_{\boldsymbol{k}_1}$ and $v_{\boldsymbol{k}_2} v^\dagger_{\boldsymbol{k}_4}$ can be neglected, excitons can be approximated as pure bosons. However, the basic constituents of excitons are fermions and at elevated densities of electrons and holes, the commutator acquires correction terms of the order $\mathcal{O}(n_x a_B^2)$ and higher, n_x being the exciton density and a_B being the excitonic Bohr radius ($a_B \sim 1$ nm, in the case of monolayer TMDs).

Now, by employing the *identity operator method* originally introduced by Ivanov and Haug [43] we may transfer purely electronic quantities to the pair-operator picture as follows [42]

$$c^\dagger_{\boldsymbol{k}_1} c_{\boldsymbol{k}_2} \approx \sum_{\boldsymbol{k}_3} P^\dagger_{\boldsymbol{k}_1,\boldsymbol{k}_3} P_{\boldsymbol{k}_2,\boldsymbol{k}_3} - \frac{1}{2} \sum_{\boldsymbol{k}_3,\boldsymbol{k}_4,\boldsymbol{k}_5} P^\dagger_{\boldsymbol{k}_1,\boldsymbol{k}_3} P^\dagger_{\boldsymbol{k}_4,\boldsymbol{k}_5} P_{\boldsymbol{k}_4,\boldsymbol{k}_5} P_{\boldsymbol{k}_2,\boldsymbol{k}_3} \ , \tag{2.26}$$

and

$$v_{\boldsymbol{k}_1} v^\dagger_{\boldsymbol{k}_2} \approx \sum_{\boldsymbol{k}_3} P^\dagger_{\boldsymbol{k}_3,\boldsymbol{k}_1} P_{\boldsymbol{k}_3,\boldsymbol{k}_2} - \frac{1}{2} \sum_{\boldsymbol{k}_3,\boldsymbol{k}_4,\boldsymbol{k}_5} P^\dagger_{\boldsymbol{k}_3,\boldsymbol{k}_1} P^\dagger_{\boldsymbol{k}_4,\boldsymbol{k}_5} P_{\boldsymbol{k}_4,\boldsymbol{k}_5} P_{\boldsymbol{k}_3,\boldsymbol{k}_2} \ . \tag{2.27}$$

Formally, one has to include an infinite number of pair operator terms in the expansions above, but depending on the excitation regime it is often sufficient to just consider terms up to first order in the excitation density, which amounts to assuming $c^\dagger c \sim P^\dagger P$. Additionally, we may, by analogy with (2.20), define new excitonic operators $X^{(\dagger)}$ according to

$$P^\dagger_{\boldsymbol{k}_1,\boldsymbol{k}_2} = \sum_n X^\dagger_{n,\boldsymbol{k}_1-\boldsymbol{k}_2} \varphi^*_{n,\beta\boldsymbol{k}_1+\alpha\boldsymbol{k}_2} \ , \tag{2.28}$$

n being a sum taken over all possible exciton states, $n = 1s,2p,2s....$
Now, taking the two-band Hamiltonian, $H = H_0 + H_{e-h}$, as an example we may transform it to an excitonic Hamiltonian using the pair operators and

basis transformation above:

$$H_0 = \sum_{\boldsymbol{k}} (\epsilon^c_{\boldsymbol{k}} c^\dagger_{\boldsymbol{k}} c_{\boldsymbol{k}} - \epsilon^v_{\boldsymbol{k}} v_{\boldsymbol{k}} v^\dagger_{\boldsymbol{k}}) \approx \sum_{n,m,\boldsymbol{k},\boldsymbol{Q}} \frac{\hbar^2 \boldsymbol{k}^2}{2\mu} X^\dagger_{n,\boldsymbol{Q}} X_{m,\boldsymbol{Q}} \varphi^*_{n,\boldsymbol{k}} \varphi_{m,\boldsymbol{k}} + \sum_{n,\boldsymbol{Q}} \frac{\hbar^2 \boldsymbol{Q}^2}{2M} X^\dagger_{n,\boldsymbol{Q}} X_{n,\boldsymbol{Q}} \ ,$$

$$H_{e-h} = \sum_{\boldsymbol{k},\boldsymbol{k'},\boldsymbol{q}} V^{cvvc}_{\boldsymbol{q}} c^\dagger_{\boldsymbol{k}+\boldsymbol{q}} v^\dagger_{\boldsymbol{k'}-\boldsymbol{q}} v_{\boldsymbol{k'}} c_{\boldsymbol{k}} \approx - \sum_{\boldsymbol{Q},\boldsymbol{q},\boldsymbol{k},n} V^{cvvc}_{\boldsymbol{q}} X^\dagger_{n,\boldsymbol{Q}} X_{m,\boldsymbol{Q}} \varphi^*_{n,\boldsymbol{k}+\boldsymbol{q}} \varphi_{m,\boldsymbol{k}} \ .$$

By forming the sum $H = H_0 + H_{e-h}$ and making use of the Wannier equation, (2.22), we deduce that

$$H_0 + H_{e-h} \approx \sum_{n,m,\boldsymbol{Q},\boldsymbol{k}} \underbrace{\left(\frac{\hbar^2 \boldsymbol{k}^2}{2\mu} \varphi^*_{n,\boldsymbol{k}} - \sum_{\boldsymbol{q}} V^{cvvc}_{\boldsymbol{q}} \varphi^*_{n,\boldsymbol{k}+\boldsymbol{q}} \right)}_{= E_n \varphi^*_{n,\boldsymbol{k}}} \varphi_{m,\boldsymbol{k}} X^\dagger_{n,\boldsymbol{Q}} X_{m,\boldsymbol{Q}} + \sum_{n,\boldsymbol{Q}} \frac{\hbar^2 \boldsymbol{Q}^2}{2M} X^\dagger_{n,\boldsymbol{Q}} X_{n,\boldsymbol{Q}} \ ,$$

simplifying to

$$H_{x,0} = \sum_{n,\boldsymbol{Q}} E^n_{\boldsymbol{Q}} X^\dagger_{n,\boldsymbol{Q}} X_{n,\boldsymbol{Q}} \ , \tag{2.29}$$

where we define the *excitonic center-of-mass dispersion*

$$E^n_{\boldsymbol{Q}} = E_n + \frac{\hbar^2 \boldsymbol{Q}^2}{2M} \ . \tag{2.30}$$

Now, by commuting our new Hamilton operator (2.29) with the excitonic polarisation $P_{n,\boldsymbol{Q}} \equiv \langle X^\dagger_{n,\boldsymbol{Q}} \rangle$ we directly obtain (2.21) (upon setting the band gap $E_g = 0$). Similarly, as outlined in detail in [42], the carrier-carrier contributions can be transformed accordingly and included in the excitonic Hamiltonian, which can be used as basis for treating exciton-exciton interactions. This gives the starting-point of the theoretical framework introduced in Paper I and is discussed further in the following chapter. Having microscopic access to the excitonic Hamiltonian now enables us to find equations of motion for excitonic observables in a straight-forward manner.

CHAPTER 3

EXCITON-EXCITON INTERACTIONS

Although a plethora of non-linear quantum phenomena in two-dimensional semiconductors, ranging from anomalous diffusion and non-conventional exciton transport [25, 36, 71] to optical non-linearities [72, 73], are attributed to exciton-exciton interactions, finding a microscopic theory of these many-body interactions has remained challenging [26, 74, 75]. In this chapter, we outline two different ways of treating exciton-exciton interactions in transition-metal dichalcogenide monolayers and heterobilayers. The first way relies on expressing the electron-electron Hamiltonian directly in terms of excitonic operators resulting in a bosonic four-operator Hamiltonian which we use in Paper I to study intra- and intervalley exciton-exciton scattering. In the second way, discussed in Paper III, we derive a *mean-field* exciton-exciton Hamiltonian to study density-dependent energy renormalizations and exciton line-shifts. Importantly and regardless of approach, we shall see that different types of excitons interact in fundamentally different ways as shown in Fig. 3.1(a): intralayer excitons in a monolayer interact through quantum-mechanical exchange interactions due to their fermionic substructure and interlayer excitons in a bilayer can be viewed as repelling dipoles.

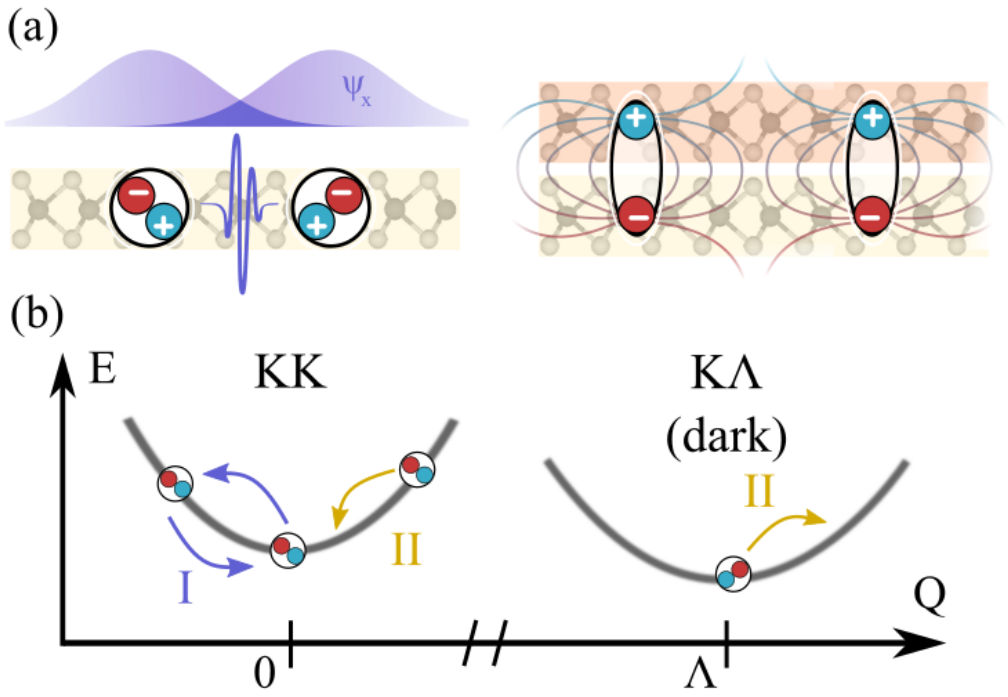

Figure 3.1: Schematic illustration of exciton-exciton interactions in a TMD monolayer and van der Waals heterostructure. (a) Intralayer excitons mainly interact through quantum-mechanical exchange interactions, with the interaction strength being crucially dependent on the excitonic wave function overlaps. In contrast, interlayer excitons exhibit a permanent out-of-plane dipole moment. (b) Dominating exciton-exciton scattering channels in an exemplary monolayer WSe_2. We distinguish between intravalley (I, purple) and intervalley (II, yellow) scattering processes. Figure taken from Ref. [76] (Paper I).

3.1 Exciton-exciton Hamiltonian

In order to describe exciton-exciton interactions on a microscopic and material-specific footing, we start out from the two-band electron-electron Hamiltonian, Eq. (2.7). In fact, we can use this Hamiltonian to study both intravalley *and* a specific type of intervalley exciton-exciton scattering which only allows for small momentum transfer $\boldsymbol{q}$, illustrated in Fig. 3.1(b). Then, by employing the pair operator expansions in (2.26) and (2.27) directly to the carrier-carrier Hamiltonian (only keeping terms which scales quadratically

with the exciton density) and transforming to the exciton basis according to (2.20) we find an approximate exciton-exciton Hamiltonian reading

$$H_{x-x} = \frac{1}{2} \sum_{\substack{\mu,\nu \\ \boldsymbol{Q},\boldsymbol{Q'},\boldsymbol{q}}} G^{\mu\nu\nu\mu}_{\boldsymbol{q}} X^{\dagger}_{\mu,\boldsymbol{Q}+\boldsymbol{q}} X^{\dagger}_{\nu,\boldsymbol{Q'}-\boldsymbol{q}} X_{\nu,\boldsymbol{Q'}} X_{\mu,\boldsymbol{Q}} \ , \tag{3.1}$$

where $X^{(\dagger)}$ are bosonic[1] creation and annihilation operators and μ and ν are compound indices which hold the exciton state $n = 1s$,$2s$... and valley $\xi = \mathrm{KK}, \mathrm{KK}', \mathrm{K}\Lambda$... (by convention, the first letter denotes the hole valley and the second letter denotes the electron valley). In Paper I, we only considered excitons in the ground state $n = 1s$, as these states are the most occupied, so for simplicity we may think of μ as a valley index, such that the *excitonic* Coulomb matrix element G describes an intravalley (intervalley) scattering process for $\mu = \nu$ ($\mu \neq \nu$) corresponding to the process I (II) in Fig. 3.1(b). The excitonic Coulomb matrix element reads

$$G^{\mu\nu\nu\mu}_{\boldsymbol{q}} = \mathcal{V}^{\mu\nu\nu\mu}_{\boldsymbol{q}} + 2\mathcal{U}^{\mu\nu\nu\mu}_{\boldsymbol{q}} \ , \tag{3.2}$$

where $\mathcal{V}^{\mu\nu\nu\mu}_{\boldsymbol{q}}$ is referred to as the *direct* exciton-exciton interaction and $\mathcal{U}^{\mu\nu\nu\mu}_{\boldsymbol{q}}$ is the *exchange* exciton-exciton interaction. As these interactions depend crucially on the *screened* Coulomb interaction matrix elements $V^{cccc}, V^{vvvv}, V^{cvvc}$ (intraband elements) and V^{cvcv} (interband element), their explicit form differ depending on whether interactions between intralayer excitons in a monolayer or interlayer excitons in a bilayer are considered. Both cases are therefore discussed separately below.

[1]This might sound surprising as the fermionic substructure has to be taken into account for excitonic operators at elevated densities, as is reflected by the *cobosonic* commutator relation in (2.25). However, by commuting the exciton-exciton interaction with the excitonic polarisation in a cobosonic and a bosonic way, and including the cobosonic correction terms in the interaction matrix elements so that the two approaches coincide, we consistently capture the fermionic nature of excitons and can use bosonic commutator relations when evaluating equations of motion using (3.1) [42].

3.2 Exciton-exciton interactions in TMD monolayers

In the case of TMD monolayers, we may approximate $V_{\boldsymbol{q}}^{\lambda\bar{\lambda}\bar{\lambda}\lambda} \approx V_{\boldsymbol{q}}$ (Eq. (2.10)) dependent on the dielectric function $\varepsilon_{\boldsymbol{q}}$ taking into account screening from the surrounding substrate and TMD layer itself, cf. Eq. (2.11). Within these approximations we find the direct part of the exciton-exciton interaction as

$$\mathcal{V}_{\boldsymbol{q}}^{\mu\nu\nu\mu} = V_{\boldsymbol{q}}\Big(F_{\mu\mu}(\beta^{\mu}\boldsymbol{q}) - F_{\mu\mu}(-\alpha^{\mu}\boldsymbol{q})\Big)\Big(F_{\nu\nu}(\beta^{\nu}\boldsymbol{q}) - F_{\nu\nu}(-\alpha^{\nu}\boldsymbol{q})\Big)^{*} , \quad (3.3)$$

where we defined the form-factors $F_{\mu\mu}(x\boldsymbol{q}) = \sum_{\boldsymbol{k}} \varphi^{*}_{\mu,\boldsymbol{k}}\varphi_{\mu,\boldsymbol{k}+x\boldsymbol{q}}$, dependent on the excitonic wave functions as obtained from the Wannier equation (Eq. (2.22)) and the electron and hole masses through $\beta = \frac{m_e}{m_e+m_h}$ and $\alpha = \frac{m_h}{m_e+m_h}$. Intriguingly, we note that this part of the interaction gets boosted by increasing the mass asymmetry of the electronic constituents forming the scattering excitons, as shown in Fig. 3.2(a). In particular, considering scattering between KK and KΛ excitons (process II in Fig. 3.1(b)), we obtain a more efficient scattering due to the large mass asymmetry between holes at the K-point and electrons at the Λ-point. By expanding Eq. (3.3) for small momentum and expressing the form-factors in real space via a Fourier transform we can get more insights in the direct matrix element:

$$\mathcal{V}_{\boldsymbol{q}}^{\mu\nu\nu\mu} \approx V_{\boldsymbol{q}} r_{\mu,B}^2 r_{\mu,B}^2 q^4 Q_{\mu} Q_{\nu} \text{ (for small } q) . \quad (3.4)$$

Here, we introduced the *effective exciton charge*

$$Q_{\mu} = \frac{m^{\mu_e} - m^{\mu_h}}{m^{\mu_e} + m^{\mu_h}} , \quad (3.5)$$

and the exciton Bohr radius $r_{\mu,B}^2 = \langle\mu|r^2|\mu\rangle$. From Eq. (3.4) we note that the direct interaction for monolayers is vanishing for $q = 0$ and that the nature of the interaction is either repulsive or attractive depending on the excitonic charge. Note that Q_{μ} should not be thought of as a charge in the electromagnetic sense, but a large imbalance in electron and hole masses polarizes the excitons to effectively become less neutral, making them interact stronger.

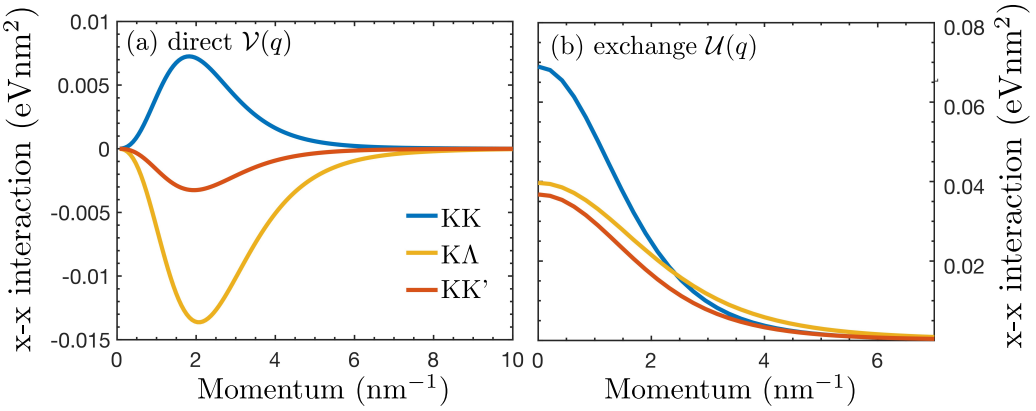

Figure 3.2: Intravalley (KK, blue) and intervalley (KK', red, KΛ, yellow) exciton-exciton interactions in an exemplary WSe_2 monolayer. Figure adapted from Ref. [76] (Paper I).

Continuing to the exchange part of the interaction we find that it, in contrast to the direct interaction, is always repulsive and non-vanishing for $q = 0$ as is typical for an exchange interaction [26]:

$$\mathcal{U}_{\boldsymbol{q}}^{\mu\nu\nu\mu} = \frac{1}{2}(\delta_{\mu_h,\nu_e}\hat{\mathcal{U}}_{\boldsymbol{q}}^{\mu\nu} + \delta_{\nu_h,\mu_e}\hat{\mathcal{U}}_{-\boldsymbol{q}}^{\nu\mu}) \ , \tag{3.6}$$

with $\hat{\mathcal{U}}_{\boldsymbol{q}}^{\mu\nu} = \sum_{\boldsymbol{q}_1,\boldsymbol{q}_2} \bar{V}_{\boldsymbol{q}_2-\boldsymbol{q}_1}^{\mu\nu} R_\mu(\boldsymbol{q}_1, \alpha^\mu \boldsymbol{q}) R_\nu(\boldsymbol{q}_2, \beta^\nu \boldsymbol{q})$ introducing $R_\mu(\boldsymbol{q}_1, x\boldsymbol{q}) = \varphi^*_{\mu,\boldsymbol{q}_1}\varphi_{\mu,\boldsymbol{q}_1+x\boldsymbol{q}}$ and the interband Coulomb interaction $\bar{V}_{\boldsymbol{q}}^{\mu\nu} = V_{\boldsymbol{q}}(\boldsymbol{q}\cdot\boldsymbol{M}_{\mu_h})(\boldsymbol{q}\cdot\boldsymbol{M}_{\nu_e})^*$ with M being the optical matrix element (cf. Section 2.1). As shown in Fig. 3.2(b), the exchange interaction strength dominates over the direct interaction strength in TMD monolayers by almost an order of magnitude. Moreover, it is not as sensitive in changes in electron and hole masses as the direct interaction.

3.3 Exciton-exciton interactions in van der Waals heterostructures

When stacking two or more transition-metal dichalcogenide monolayers together we obtain a van der Waals heterostructure, which enables the for-

mation of long-lived interlayer excitons, i.e. excitons composed of electrons and holes in different layers [77] . Due to the increased dielectric screening from the other layer, interlayer exciton binding energies are smaller than the exciton binding energies in a monolayer. In particular, considering KK interlayer excitons in hBN-encapsulated $MoSe_2$-WSe_2 we deduce a binding energy of around 90 meV [76], differing a factor two from the intralayer binding energies in monolayer WSe_2, cf. Fig. 2.2. Still, due to the type-II band alignment in $MoSe_2$-WSe_2 [78], the KK interlayer exciton state is rendered by far the energetically lowest state and hence it is expected that interlayer exciton-exciton interactions play a vital role in this particular heterostructure. By introducing layer indices l and $\bar{l}$ such that $V_{\boldsymbol{q}}^{cccc} \to V_{\boldsymbol{q}}^{c_l c_l c_l c_l} = \frac{V_{\text{bare},\boldsymbol{q}}}{\varepsilon_{\boldsymbol{q}}^{ll}}$, $V_{\boldsymbol{q}}^{vvvv} \to V_{\boldsymbol{q}}^{v_{\bar{l}} v_{\bar{l}} v_{\bar{l}} v_{\bar{l}}} = \frac{V_{\text{bare},\boldsymbol{q}}}{\varepsilon_{\boldsymbol{q}}^{ll}}$ and $V_{\boldsymbol{q}}^{c_l v_{\bar{l}} v_{\bar{l}} c_l} = \frac{V_{\text{bare},\boldsymbol{q}}}{\varepsilon_{\boldsymbol{q}}^{ll}}$, with layer-dependent dielectric functions [35, 79], the direct exciton-exciton interaction, which previously just included interactions between intralayer excitons (abbreviated X-X), is generalized to interlayer exciton-exciton interactions (IX-IX) and intralayer-interlayer interactions (IX-X) . Here, we will not provide the full lengthy expressions for the corresponding X-X, IX-X or IX-IX interactions, but in analogy to (3.4) consider the small q limit. In this case, we find

$$\mathcal{V}_{\boldsymbol{q}}^{\text{IX}-\text{IX}} = \frac{e^2}{2\epsilon_0}\left(\frac{d_1}{\varepsilon_{\perp}^{(1)}} + \frac{d_2}{\varepsilon_{\perp}^{(2)}}\right) + \mathcal{O}(\boldsymbol{q}) \text{ (for small } q) \text{ ,} \tag{3.7}$$

where d_i are the TMD layer thicknesses and $\varepsilon_{\perp}^{(i)}$ are perpendicular components of the dielectric tensor of the TMDs $i = 1,2$, the latter being extracted from DFT calculations [80]. By inspection, the direct interlayer exciton-exciton interaction is a dipole-dipole interaction, where the layer thicknesses d_i determine the separation between electrons and holes and thereby the out-of-plane dipole moment of the interlayer excitons. Similarly, one finds that the interaction between intralayer excitons in a heterostructure, $\mathcal{V}_{\boldsymbol{q}}^{\text{X}-\text{X}}$, scales with q^2 as in the monolayer case, and that the mixed interaction between intra- and interlayer excitons, $\mathcal{V}_{\boldsymbol{q}}^{\text{X}-\text{IX}}$ attains a constant value in the limit $q \to 0$, reflecting the permanent out-of-plane dipole moment of the IX. The full momentum-dependent matrix elements are shown in Fig. 3.3, revealing a strong repulsive interaction for all q for the IX-IX and IX-X interactions, reflecting the dipolar nature of interlayer excitons. Moreover, due to the spatial separation of electrons and holes forming the interlayer exciton in a heterostructure, their optical matrix element is suppressed, and consequently the corresponding exchange contribution $\mathcal{U}$ is negligible. The exciton-exciton

Hamiltonian in (3.1) enables us to study scattering processes between different species of excitons. However, special care has to be taken when deriving equations of motion using (3.1). In particular, considering the equation of motion for the exciton polarisation $\langle X^\dagger_{\mu,\boldsymbol{Q}}\rangle$ we deduce that

$$\frac{d}{dt}\langle X^\dagger_{\mu,\boldsymbol{Q}}\rangle|_{H_{x-x}} = \frac{i}{\hbar}\sum_{\nu,\boldsymbol{Q'},\boldsymbol{q}} G^{\mu\nu\nu\mu}_{\boldsymbol{q}}\langle X^\dagger_{\mu,\boldsymbol{Q}+\boldsymbol{q}}X^\dagger_{\nu,\boldsymbol{Q'}-\boldsymbol{q}}X_{\nu,\boldsymbol{Q'}}\rangle\ . \tag{3.8}$$

The polarisation couples back to a three-operator quantity which needs to be factorized into the corresponding Hartree and Fock terms (cf. Section 2.2) and correlations, with the correlations giving rise to Boltzmann-like exciton-

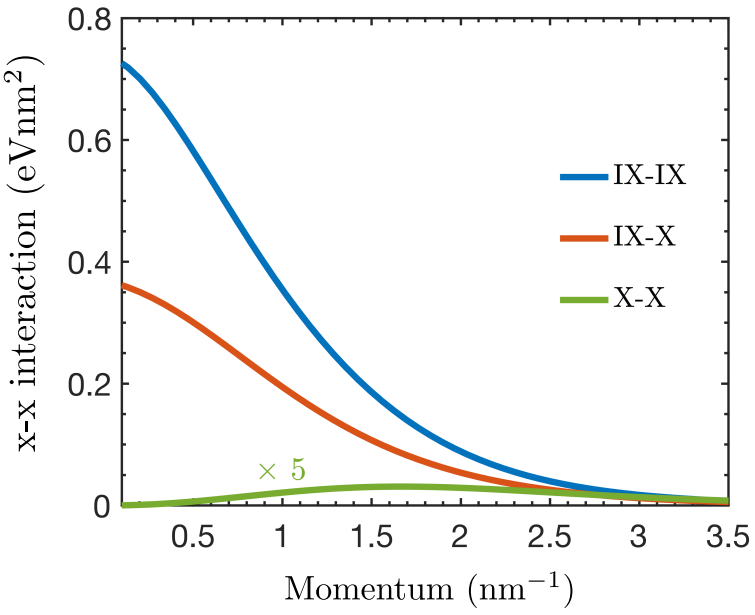

Figure 3.3: Interlayer (IX) and intralayer (X) exciton-exciton interactions in $MoSe_2$-WSe_2 heterostructures. Momentum space representation of the direct dipole-dipole interaction. Interlayer excitons exhibit a permanent out-of-plane dipole moment and hence interact much stronger than intralayer excitons. Figure adapted from Ref. [76] (Paper I).

exciton scattering equations[2]. In Paper I, a completely bosonic treatment of the scattering is made, but formally the cluster expansion for the multi-operator excitonic quantity $\langle X^\dagger X^\dagger ....\rangle$ has to respect individual exchanges of electrons and holes, which is not captured by a purely bosonic factorization scheme. As it is cumbersome to include these exchange terms properly in the factorization scheme, we in the following introduce and derive a simplified mean-field exciton-exciton Hamiltonian that explicitly includes these effects.

3.4 Mean-field exciton-exciton Hamiltonian

Here we derive a Hamiltonian which can be used to study exciton-exciton interactions on a *mean-field* level as done in Paper III. Instead of directly transforming the carrier-carrier Hamiltonian (Eq. (2.7)) to the exciton basis and arrive at a four-operator exciton-exciton Hamiltonian expressed in terms of excitonic operators $X^{(\dagger)}$, we here construct a two-operator Hamiltonian starting from the equation of motion for the microscopic polarisation, $p_{\boldsymbol{k},\boldsymbol{k'}}$, in electron-hole picture (Eq. (2.16)). For simplicity, we assume a system which is dominated by excitons with one specific valley-configuration, which is typically the case at low temperatures. The equation of motion for the polarisation can be transformed to the excitonic basis, so that $p_{\boldsymbol{k},\boldsymbol{k'}} \to P_{n,\boldsymbol{Q}}$, and making use of the pair operator expansions (2.26) and (2.27), yielding the following equation:[3]

$$\begin{aligned}\dot{P}_{n,\boldsymbol{Q}} = \frac{i}{\hbar}\Bigg(&(E^n_{\boldsymbol{Q}} + \sum_{\boldsymbol{q}} V^{vv}_{\boldsymbol{q}}) P_{n,\boldsymbol{Q}} \\ &+ \sum_{\substack{\boldsymbol{k},\boldsymbol{k'},\boldsymbol{q},\boldsymbol{Q'} \\ i,j,m}} P_{m,\boldsymbol{Q}-\boldsymbol{q}} N^{ij}_{\boldsymbol{Q'}+\boldsymbol{q},\boldsymbol{Q'}} (\mathcal{V}^{imnj}_{\boldsymbol{q}} + \mathcal{E}^{imnj}_{\boldsymbol{k},\boldsymbol{k'},\boldsymbol{Q},\boldsymbol{Q'},\boldsymbol{q}})\Bigg) ,\end{aligned} \tag{3.9}$$

[2]In Paper I, we make use of the resulting scattering equations to study *excitation-induced dephasing*, an experimentally accessible phenomenon which becomes manifest as density-dependent broadenings in excitonic transitions [72]. See details in Ref. [76].

[3]Here, we decided to include also the contributions stemming from interband Coulomb interaction which are proportional to $N_{\boldsymbol{Q'}+\boldsymbol{q},\boldsymbol{Q'}}$. The interband Coulomb interaction also gives rise to a linear term in $P_{n,\boldsymbol{Q}}$ which scales as $\bar{V}^{cv}_{\boldsymbol{Q}} \sum_{m,\boldsymbol{k},\boldsymbol{k'}} \varphi^*_{m,\boldsymbol{k}} \varphi_{n,\boldsymbol{k'}}$ and modifies the free exciton dispersion $E^n_{\boldsymbol{Q}}$. This term is not of our interest here, but is discussed in other works [30, 81, 82].

where i,j,m,n = 1s,2p,2s... is the excitonic state and where we introduced $N^{ij}_{\boldsymbol{Q},\boldsymbol{Q'}} = \langle X^{\dagger}_{i,\boldsymbol{Q}} X_{j,\boldsymbol{Q'}} \rangle$ and were able to identify the *direct* exciton-exciton interaction, $\mathcal{V}^{imnj}_{\boldsymbol{q}}$, Eq. (3.3). We also adapted the shorthand notation $V^{cccc} \equiv V^{cc}$, $V^{vvvv} \equiv V^{vv}$ and $V^{cvvc} \equiv V^{cv}$ for the screened intraband Coulomb interactions here and $\bar{V}^{cv} \equiv V^{cvcv}$ for the interband Coulomb interaction. The remaining terms can be summarized in a single *exchange* term

$$\begin{aligned}
\mathcal{E}^{imnj}_{\boldsymbol{k},\boldsymbol{k'},\boldsymbol{Q},\boldsymbol{Q'},\boldsymbol{q}} = &(V^{cv}_{\boldsymbol{k}-\boldsymbol{k'}}\varphi_{n,\boldsymbol{k'}} - V^{cc}_{\boldsymbol{k}-\boldsymbol{k'}}\varphi_{n,\boldsymbol{k}})\times \\
&\varphi^{*}_{i,\boldsymbol{k'}+\beta(\boldsymbol{Q'}+\boldsymbol{q}-\boldsymbol{Q})}\varphi_{j,\boldsymbol{k'}+\beta(\boldsymbol{Q'}+\boldsymbol{q}-\boldsymbol{Q})+\alpha\boldsymbol{q}}\varphi^{*}_{m,\boldsymbol{k}+\alpha\boldsymbol{q}} \\
&+ (V^{cv}_{\boldsymbol{k}-\boldsymbol{k'}}\varphi_{n,\boldsymbol{k'}} - V^{vv}_{\boldsymbol{k}-\boldsymbol{k'}}\varphi_{n,\boldsymbol{k}})\times \\
&\varphi^{*}_{i,\boldsymbol{k'}-\alpha(\boldsymbol{Q'}+\boldsymbol{q}-\boldsymbol{Q})}\varphi_{j,\boldsymbol{k'}-\alpha(\boldsymbol{Q'}+\boldsymbol{q}-\boldsymbol{Q})-\beta\boldsymbol{q}}\varphi^{*}_{m,\boldsymbol{k}-\beta\boldsymbol{q}} \\
&+ \bar{V}^{cv}_{\boldsymbol{k}-\boldsymbol{k'}}\varphi^{*}_{i,\boldsymbol{k'}-\beta\boldsymbol{Q}-\alpha\boldsymbol{Q'}+\beta\boldsymbol{q}}\varphi_{j,\boldsymbol{k'}-\beta\boldsymbol{Q}-\alpha\boldsymbol{Q'}}\varphi^{*}_{m,\boldsymbol{k}+\alpha\boldsymbol{q}}\varphi_{n,\boldsymbol{k}} \\
&+ \bar{V}^{cv}_{\boldsymbol{k}-\boldsymbol{k'}}\varphi^{*}_{i,\boldsymbol{k'}+\beta\boldsymbol{Q'}+\alpha\boldsymbol{Q}-\alpha\boldsymbol{q}}\varphi_{j,\boldsymbol{k'}+\beta\boldsymbol{Q'}+\alpha\boldsymbol{Q}}\varphi^{*}_{m,\boldsymbol{k}-\beta\boldsymbol{q}}\varphi_{n,\boldsymbol{k}} \ .
\end{aligned} \tag{3.10}$$

Here, the first two terms corresponds to electron-electron exchange, the third and fourth terms takes into account hole-hole exchange respectively [26, 83]. The final terms are due to interband electron-hole interactions [84]. Note that the contributions from electron-electron/hole-hole and electron-hole interactions to the exchange interaction come with opposite signs. This reflects the attractive (repulsive) nature of the electron-hole (electron-electron/hole-hole) interactions.

Due to the dependence on many momenta, the exchange interaction is generally not easily evaluated. However, as the center-of-mass momenta $\boldsymbol{Q}^{(\prime)}$ are typically of the order of the thermal wave vector, i.e. $\boldsymbol{Q}^{(\prime)} \sim \sqrt{\frac{2Mk_BT}{\hbar^2}}$, T being temperature and M being the total exciton mass and the exciton relative momenta $\boldsymbol{k}^{(\prime)} \sim a_B^{-1}$ with the inverse exciton Bohr radius a_B^{-1} it follows that $\boldsymbol{Q}$,$\boldsymbol{Q'} << \boldsymbol{k}^{(\prime)}$, the center-of-mass momentum dependence is usually neglected in the matrix elements. In particular, it then holds that $\sum_{\boldsymbol{k},\boldsymbol{k'}} \mathcal{E}^{imnj}_{\boldsymbol{k},\boldsymbol{k'},\boldsymbol{Q'},\boldsymbol{Q},\boldsymbol{q}}|_{\text{interb.}} \approx \mathcal{U}^{imnj}_{\boldsymbol{q}}$, i.e. we have recovered the exchange contribution in (3.6). However, in contrast to in the previous section, we now also have contributions to the exchange interaction stemming from the intraband Coulomb interaction including exchange of individual electrons or holes. Now, we define the *mean-field exciton-exciton interaction*

$$G^{mn}_{\boldsymbol{Q},\boldsymbol{q}} = \sum_{\boldsymbol{k},\boldsymbol{k'},i,j,\boldsymbol{Q'}} N^{ij}_{\boldsymbol{Q'}+\boldsymbol{q},\boldsymbol{Q'}} \left(\mathcal{V}^{imnj}_{\boldsymbol{q}} + \mathcal{E}^{imnj}_{\boldsymbol{k},\boldsymbol{k'},\boldsymbol{Q},\boldsymbol{Q'},\boldsymbol{q}} \right) , \tag{3.11}$$

enabling us to construct the two-operator exciton-exciton Hamiltonian

$$H_{x-x,\mathrm{mf}} = \sum_{\boldsymbol{Q},\boldsymbol{q},,n,m} G^{mn}_{\boldsymbol{Q},\boldsymbol{q}} X^{\dagger}_{m,\boldsymbol{Q}-\boldsymbol{q}} X_{n,\boldsymbol{Q}} \ , \tag{3.12}$$

which together with the free Hamiltonian[4] (2.29) and commutation with the excitonic polarisation $P_{n,\boldsymbol{Q}} = \langle X^{\dagger}_{n,\boldsymbol{Q}} \rangle$ gives rise to the equation of motion (3.9).

3.5 Density-dependent line shifts

Having access to the mean-field exciton-exciton Hamiltonian simplifies the calculation of *density-dependent* exciton line shifts drastically and enables us to disentangle the different interaction mechanisms contributing to experimentally measured intralayer redshifts and interlayer blueshifts with pump power in TMD monolayers and TMD heterobilayers, respectively. The experimentally observed blue-shift with pump power for the interlayer exciton peak, is commonly attributed to strong repulsive dipole-dipole interactions [36, 73], but here we also display the importance of exchange interactions. Moreover, at elevated electron-hole densities, excitons screen each other[5] [86], in analogy to how electrons or holes screen each other in a semiconductor [87], which induces a density-dependence in the interaction matrix elements as well as in the electronic band gap. Taking this fact into account and considering the equation of motion for bright ($\boldsymbol{Q} = 0$) $n = 1s$ excitons within a rotating wave approximation, Eq. (3.9) is simplified to

$$\dot{P}_{1s} = \frac{i}{\hbar}\Big(E_{1s} + \Delta E(n_x) \Big) \ , \tag{3.13}$$

where E_{1s} is the KK $1s$ exciton binding energy, $n_x = \sum_{\boldsymbol{Q}} N_{\boldsymbol{Q}}$ is the exciton density and, importantly, $\Delta E(n_x)$ is the density-dependent energy renormalization:

$$\Delta E(n_x) = (g_{d-d} + g_{x-x}) n_x - \Sigma_{CH} \ . \tag{3.14}$$

[4]Here we absorbed the term $\sum_{\boldsymbol{q}} V^{vv}_{\boldsymbol{q}}$ in the center-of-mass dispersion, as it just renormalizes the electronic band gap.

[5]At densities below the *Mott transition* at which excitons are dissociated into a liquid or plasma of electrons and holes [85], it is expected that most electrons and holes are bound as excitons.

Here, $g_{d-d} = \delta_{\boldsymbol{q},0}\mathcal{V}_{\boldsymbol{q}}^{1s-1s}$ is the dipole-dipole interaction evaluated at $\boldsymbol{q} = 0$ which is vanishing for intralayer excitons in a TMD monolayer (Cf. Eq. (3.4) and Fig. 3.2) and non-zero when considering interactions between interlayer excitons in a van der Waals heterostructure (Cf. Eq. (3.7) and Fig. 3.3). The exchange interaction g_{x-x} is obtained as $g_{x-x} \approx \sum_{\boldsymbol{k},\boldsymbol{k'}} \mathcal{E}^{1s-1s}_{\boldsymbol{k},\boldsymbol{k'},0,0,0}$ and reads

$$\begin{aligned} g_{x-x} = &\sum_{\boldsymbol{k},\boldsymbol{k'}} \varphi^*_{\boldsymbol{k'}}\varphi_{\boldsymbol{k'}}(2V^{cv}_{\boldsymbol{k}}\varphi^*_{\boldsymbol{k}+\boldsymbol{k'}}\varphi_{\boldsymbol{k'}} - V^{cc}_{\boldsymbol{k}}|\varphi_{\boldsymbol{k'}+\boldsymbol{k}}|^2 - V^{vv}_{\boldsymbol{k}}|\varphi_{\boldsymbol{k'}+\boldsymbol{k}}|^2) \\ &+ 2\sum_{\boldsymbol{k},\boldsymbol{k'}} \bar{V}^{cv}_{\boldsymbol{k}-\boldsymbol{k'}}|\varphi_{\boldsymbol{k}}|^2|\varphi_{\boldsymbol{k'}}|^2 \ . \end{aligned} \tag{3.15}$$

By inspection of the expression above, it is not clear whether the interaction is repulsive or attractive. However, in a TMD monolayer we may approximate $V^{cv} \approx V^{cc} \approx V^{vv} \approx V$ where V is the screened Keldysh-like Coulomb potential.[6] In contrast, considering interactions between electrons and holes in different TMD layers, we note that $V^{cv} << V^{cc}, V^{vv}$ (due to increased screening between layers) and the electron-hole interaction is highly sensitive with respect to the layer separation. Moreover, the interband contribution to the interlayer exchange interaction ($\propto \bar{V}^{cv}$) is negligible, due to the suppressed optical matrix element of spatially separated charges [90]. As such, we find that g_{x-x} is in general attractive for interlayer excitons and repulsive for intralayer excitons. Finally, we introduced the *Coulomb-hole term* in (3.14) which includes density-dependent effects of the electronic band gap [91]. This term reads $\Sigma_{CH} = \sum_{\boldsymbol{q}}(V^{vv}_{\boldsymbol{q}} - \frac{V^{vv}_{\boldsymbol{q}}}{\epsilon_{\text{exc},\boldsymbol{q}}(n_x)})$, where $\epsilon_{\text{exc},\boldsymbol{q}}(n_x)$ is the excitonic screening obtained via a static excitonic Lindhard model (details in Paper III).

In Fig. 3.4, we show the density dependence of the energy renormalization, ΔE, (3.14) for intralayer excitons (X) in a WSe_2 monolayer and interlayer

[6] In fact, the intralayer exchange interaction can be analytically evaluated assuming an *unscreened* Coulomb potential (Eq. (2.10)) and hydrogen-like wave functions, as $g_{x-x} \propto E_{1s}a_B^2$, a_B being the exciton Bohr radius [83, 88]. A generalization of the exchange interaction to higher-lying exciton states is found in [89].

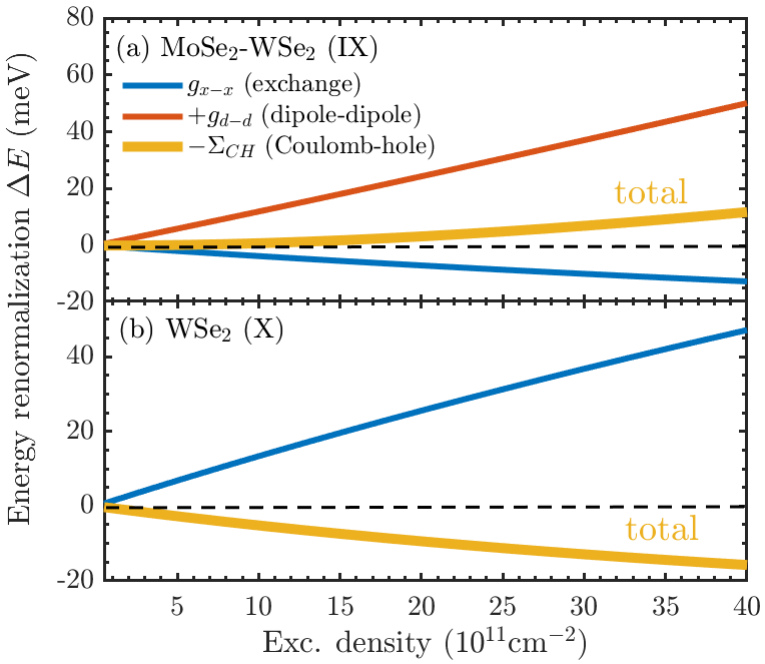

Figure 3.4: Density-dependent exciton line shifts in hBN-encapsulated $MoSe_2$-WSe_2 heterobilayers and WSe_2 monolayers respectively. Individual contributions are added up consequtively. (a) Interlayer exciton line shifts as a function of exciton density, n_x including dipole-dipole, exchange interactions and Coulomb-hole contributions. We obtain a net blue-shift of the exciton line for interlayer excitons (IX). (b) Intralayer exciton line shifts. Here we obtain a net weak red-shift of the exciton line, due to the absence of strong dipole-dipole interactions and efficient exciton screening (reflected by the Coulomb-hole term).

excitons (IX) in a $MoSe_2$-WSe_2 heterobilayer[7]. Importantly, we obtain a net blue-shift of 15 meV for interlayer excitons as a result of strong dipole-dipole interactions- in good agreement with experimental studies [73] and a similar red-shift for intralayer excitons when increasing pump power, which

[7]The heterobilayer $MoSe_2$-WSe_2 is not chosen by coincidence. Due to the large type-II band alignment between Mo- and W-layers of the order of 300 meVs depending on stacking [35], it follows that the energetically lowest state by far in this particular structure is an interlayer exciton state. As a consequence, the interlayer exciton occupation is dominant in this structure and strong dipolar exciton-exciton interactions are expected even at room temperature. In contrast, in many other structures such as homobilayers, the energetically lowest state is generally hybridised and contains contributions stemming from both intra- and interlayer excitons [92].

we explain through the interplay of Coulomb-induced repulsive and attractive interactions as discussed in detail above. Importantly, the Coulomb-hole term, which includes the mutual Coulomb repulsion between holes in the valence band, results in a significant reduction of the line shifts in both cases, and a blueshift-redshift crossover in the intralayer case. This has been verified by previous microscopic calculations for TMD monolayers [93].

In the following chapter we will investigate the role of repulsive interactions between interlayer excitons further. In particular, we find that the density-dependent energy renormalizations discussed here are of vital importance when considering the transport of excitons in real space, where $\Delta E(n_x)$ is promoted to a spatially dependent interaction potential, $\Delta E(n(x,y))$.

CHAPTER 4

ANOMALOUS INTERLAYER EXCITON TRANSPORT

Understanding and being able to control exciton transport is crucial for the efficiency of exciton-based devices [94–96]. Here, we will be concerned with the transport of interlayer excitons, i.e. excitons composed from electrons and holes in different layers in a van der Waals heterostructure. As discussed in the previous chapter, these excitons exhibit a permanent out-of-plane dipole moment and as such they display strong repulsive interactions. Recent experimental studies on heterobilayers [25, 36] report on non-linear exciton propagation and anomalous diffusion at elevated electron-hole densities and attribute this to repulsive exciton-exciton interactions, motivating us to investigate the role of these interactions on a microscopic footing. By having access to a material-specific and microscopic theory of interlayer exciton-exciton interactions we are able to provide insights on additional experimentally accessible tuning knobs when it comes to exciton transport. Our findings on this topic are found in Paper III, and are summarized briefly in this chapter.

4.1 Drift-diffusion equation for interlayer excitons

In order to be able to model exciton transport in two-dimensional semiconductors we need access to the spatiotemporal dynamics of excitons, i.e. resolve the distribution of excitons in space and time. This information is encoded in the *Wigner function* $N_{\mathbf{Q}}(\mathbf{r}) = \sum_{\mathbf{q}} \mathrm{e}^{i\mathbf{q}\cdot\mathbf{r}} \langle X^{\dagger}_{\mathbf{Q}-\mathbf{q}/2} X_{\mathbf{Q}+\mathbf{q}/2} \rangle$, which describes the quasiprobability distribution of excitons with center-of-mass momentum $\mathbf{Q}$ at position $\mathbf{r}$. Here, $X^{(\dagger)}$ are excitonic operators, as introduced in Section 2.4. Now, as outlined in detail by Hess and Kuhn [97], the spatiotemporal dynamics of excitons can be accessed by evaluating the Heisenberg equation of motion for the off-diagonal quantity $N_{\mathbf{Q},\mathbf{Q}'} \equiv \langle X^{\dagger}_{\mathbf{Q}} X_{\mathbf{Q}'} \rangle$ and Fourier-transform the result to get an equation of motion for the Wigner function [95, 98]. To take exciton-exciton interactions into account we employ the mean-field Hamiltonian introduced in Eq. (3.12), which together with the free exciton Hamiltonian (2.30) gives us the equation of motion for $N_{\mathbf{Q},\mathbf{Q}'}$. By Fourier transforming and performing a Taylor expansion with respect to momentum and space coordinates we deduce the following to lowest order

$$\dot{N}_{\mathbf{Q}}(\mathbf{r}) = -v_{\mathbf{Q}} \nabla_{\mathbf{r}} N_{\mathbf{Q}}(\mathbf{r}) - \frac{g_{IX}}{k_B T} v_{\mathbf{Q}} \cdot \nabla_{\mathbf{r}} n(\mathbf{r}) N_{\mathbf{Q}}(\mathbf{r}) \ . \tag{4.1}$$

Here, the first term describes free propagation of excitons with velocity $v_{\mathbf{Q}} = \frac{\hbar \mathbf{Q}}{M}$, M being the total exciton mass, and the second term results in a drift of interlayer excitons caused by exciton-exciton interaction $g_{IX} = g_{x-x} + g_{d-d}$, with the dipole-dipole and exchange contributions being defined in Eq. (3.7) and Eq. (3.15) respectively. It was here moreover assumed that $N_{\mathbf{Q}}(\mathbf{r}) = N_{\mathbf{Q},\mathrm{eq}} n(\mathbf{r})$, where $N_{\mathbf{Q},\mathrm{eq}}$ is an equilibrium Boltzmann distribution with temperature T and $n(\mathbf{r})$ is a spatially dependent exciton density. Next, we recognize the equation above as a Boltzmann transport equation. This enables us to invoke the relaxation time approximation, sum out the $\mathbf{Q}$-dependence and make use of the continuity equation (details spelled out in [97]) and find an equation of motion for the interlayer exciton density reading

$$\partial_t n(\mathbf{r},t) = D \nabla^2 n(\mathbf{r},t) + \mu_m \nabla \cdot (\Delta E(n(\boldsymbol{r},t)) \nabla n(\mathbf{r},t)) - \frac{n(\boldsymbol{r},t)}{\tau} \ , \tag{4.2}$$

where we introduced the diffusion coefficient $D = \frac{1}{2An_x}\sum_{\mathbf{Q}}(v_{\mathbf{Q}})^2\tau_{\mathbf{Q}}N_{\mathbf{Q},\mathrm{eq}}$, dependent on the scattering time[1] $\tau_{\mathbf{Q}}$, and the exciton mobility $\mu_m = \frac{D}{k_BT}$ following the Einstein relation. We also phenomenologically took into account the decay of interlayer excitons by including a term proportional to $1/\tau$, τ being the exciton life time. Finally, a now spatially dependent ΔE (Eq. (3.14) with $n_x \to n(\boldsymbol{r},t)$) due to exciton-exciton interactions and screening appears in Eq. (4.2).

Eq. (4.2) is commonly referred to as a *drift-diffusion* equation [99], with the first term describing the free propagation of excitons and the second term denoting the Coulomb-induced drift term. In particular, we note that exciton-exciton interactions contribute to a drift force at elevated densities of electrons and holes. A numerical evaluation of (4.2) gives us access to the space- and time-dependent exciton density and allows us to investigate the impact of exciton-exciton interactions on non-linear exciton transport further.

In Fig. 4.1 we present the spatiotemporal dynamics of interlayer excitons in an exemplary hBN-encapsulated $MoSe_2$-hBN-WSe_2 heterotrilayer. We initialize the exciton density as a Gaussian distribution, such that $n(x,y) = n_x\exp(-(x^2+y^2)/\sigma_0^2)$ with the initial peak density $n_x = 5\cdot 10^{12}$ cm^{-2} and variance (laser spot size) $\sigma_0^2 = 1$ μm^2. As time progresses the initial distribution develops into a super-Gaussian as shown in Fig. 4.1(a)-(b). Including only diffusion, i.e. the first term in (4.2), we note that the Gaussian shape is retained and the variance of the distribution varies linearly with time (Fig. 4.1 (c)), as is expected from Fick's second law [98]. However, including also exciton-exciton interactions, we deduce that the exciton transport becomes highly non-linear - a hallmark of anomalous diffusion. As the repulsive exciton-exciton interactions is reduced by exchange interactions (as a consequence of its net attractive nature for interlayer excitons, cf. Eq. (3.15)) and exciton screening, the anomalous diffusion becomes less enhanced when including all Coulomb-induced contributions to the drift term. Finally, we note that the non-linear character of the interlayer exciton transport can be crucially tuned by changing the (initial) electron-hole density n_x. As shown

[1]The scattering time can be microscopically calculated using an interlayer analogue for the exciton-phonon scattering rates for transition-metal dichalcogenides monolayers. However, in this study we take the interlayer diffusion coefficient from experimental measurements recently performed by Kis et al. [36]

in Paper III, electron-hole densities $n_x > 10^{12}$ cm^{-2} are needed in order for Coulomb-induced drift to dominate over purely diffusive propagation.

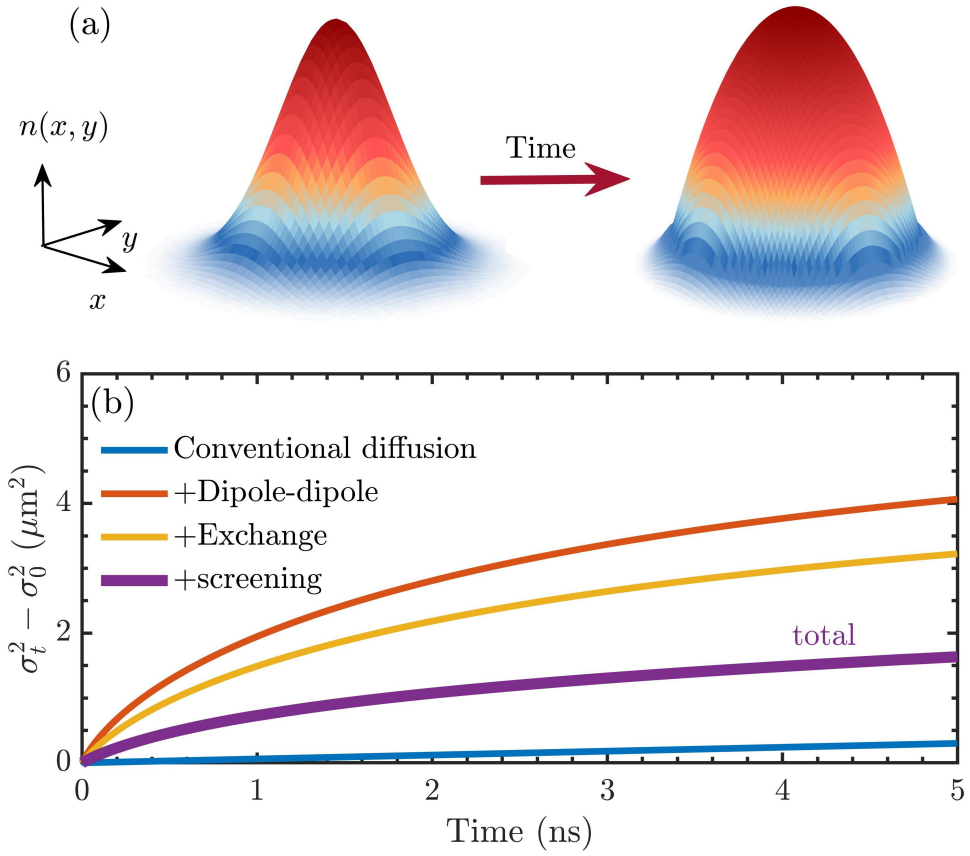

Figure 4.1: Exciton transport in $MoSe_2$-hBN-WSe_2 heterotrilayers. (a) Time evolution of exciton density $n(x,y,t)$, assuming a Gaussian distribution at $t = 0$. (b) Time-dependent variances (width of exciton density distribution), separating contributions from diffusion (blue) and different drift terms. Note that the contributions are consequtively added up. Figure adapted from Paper III.

4.2 Experimental control of interlayer exciton transport

As noted already in the previous chapter, the dominating dipole repulsion between interlayer excitons is directly proportional to the spatial separation between the electron and hole forming the interlayer exciton. This implies that the exciton-exciton interaction is highly tunable with layer separation and the interaction strength in van der Waals heterostructures can be experimentally controlled simply by including dielectric spacers between the stacked TMD monolayers. Note that we already have been considering a heterotrilayer in the transport study above, with a hBN spacer acting as a dielectric[2] between molybdenum- and tungsten-layers. In Fig. 4.2, we show the time-dependent *effective* diffusion coefficient given by the slope[3] of the variance, i.e. $D_{\text{eff}}(t) \equiv \frac{1}{4}\frac{d}{dt}\sigma_t^2$ for different number of hBN spacers between the TMD layers. For small times t we note that the obtained effective diffusion coefficient can differ more than an order of magnitude from the low density diffusion coefficient D (indicated with an orange dashed line). This reflects the overall faster propagation of interlayer excitons at elevated electron-hole densities and the importance of the interlayer exciton drift (cf. Eq. (4.2)). In particular, by increasing the number of hBN spacers between the layers, anomalous diffusion is enhanced as a consequence of increased dipole moments of interlayer excitons with layer separation (cf. the inset in Fig. 4.2). Intriguingly, we also find that the exchange interactions become more attractive as the number of hBN spacers increases, counteracting the repulsive dipole-dipole interaction. This can be explained by the interplay of electron-hole and electron-electron/hole-hole Coulomb interaction entering the exchange interaction (Eq. (3.15)), with the former being strongly suppressed when separating the charge constituents of the interlayer exciton further. As time progresses, excitons drift away from the initial laser spot and exciton density drops, and eventually conventional diffusion starts to dominate over Coulomb-induced drift, causing the effective diffusion coeffi-

[2]The inclusion of a hBN spacer between the TMD layers does not only enhance the dipole moment of interlayer excitons, but also suppresses the impact of moiré potentials which may trap excitons and affect their transport properties [71, 100].

[3]In the low density regime, where diffusion dominates over repulsive exciton-exciton interactions, Eq. (4.2) can be solved analytically and the time-dependent two-dimensional variance is given by $\sigma_t^2 = 4Dt + \sigma_0^2$.

cient to coincide with the low density diffusion coefficient $D = 0.15$ cm^2/s at $t \to \infty$. By tuning the layer separation between TMD layers we have hence shown how the non-linear character of the interlayer exciton transport can be experimentally controlled. In Paper III, we also display the importance of dielectric environment, i.e. the surrounding substrate of heterostructure, as well as the size of laser spot size when it comes to exciton diffusion. Altogether, the obtained insights are highly relevant for the development of exciton-based devices. This study paves the way for investigating exciton transport in more exotic systems such as twisted moiré materials, in which exciton states are known to be strongly hybridised and as such can be viewed as a combination of intra- and interlayer exciton states [101]. This is particularly interesting in the context of repulsive dipole-dipole interactions, as the size of hybrid out-of-plane dipole moments is expected to be highly dependent on the degree of hybridisation [102]. Moreover, the strong moiré potentials in twisted heterostructures enables trapping of excitons, which crucially could affect their transport properties [71].

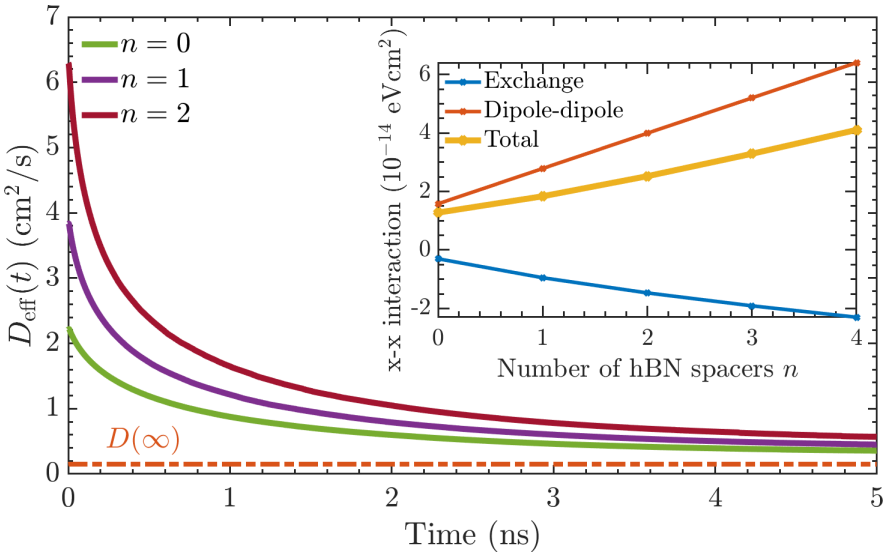

Figure 4.2: Time-dependent effective diffusion coefficient for different number of hBN spacers. The inset illustrates the dependence of the interlayer separation, $R = nd_{\text{hBN}}$ on the exciton-exciton interaction, revealing a net increase of the interaction with layer separation. Figure taken from Paper III.

CHAPTER 5

AUGER RECOMBINATION AND EXCITON-EXCITON ANNIHILATION

In this chapter, based on Paper II, we will be concerned with a particularly important process when it comes to the efficiency of optoelectronic applications, referred to as *exciton-exciton annihilation*. Exciton-exciton annihilation (EEA) is a non-radiative scattering process in which two excitons annihilate each other and form a higher-energetic exciton (HX) as schematically illustrated in Fig. 5.1 (a). As the name suggests, this process constitutes a particular type of exciton-exciton scattering. However, in contrast to the scattering processes considered in Chapter 3 and in Paper I, we here consider so-called Auger scattering processes involving three carriers.

Traditionally, Auger scattering or Auger recombination has known to be extremely efficient in e.g. graphene [103], through which an electron in the conduction band recombines with a hole in the valence band and another electron is excited further up in the conduction band. However, in the case of transition-metal dichalcogenides there are additional scattering channels available. In particular, considering tungsten-based monolayers which have a dark excitonic ground state (cf. Fig. 2.1) [104], we may distinguish between intravalley Auger recombination processes (I) and intervalley processes (II and III), cf. Fig. 5.1(b). Furthermore, due to the energetic separation of

conduction bands and the fact that the conduction and valence bands exhibit a parabolic dispersion around the high-symmetry points in these particular materials it turns out that Auger recombination processes involving two *different* conduction bands[1] [107], as shown in Fig. 5.1, are possible and, as we show in Paper II, highly efficient.

In the following, we will briefly summarize the findings in Paper II by introducing the theoretical framework for exciton-exciton annihilation and use it to evaluate the exciton-exciton annihilation rate or Auger coefficient, which is an experimentally accessible quantity. The microscopic and material-specific theory we present in this chapter has been supported and successfully confirmed by time-resolved photoluminescence measurements carried out by the group of Alexey Chernikov (TU Dresden/University of Regensburg).

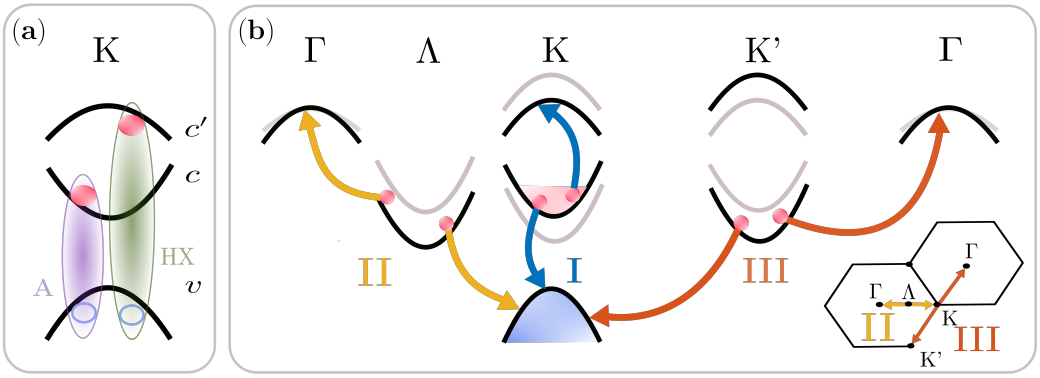

Figure 5.1: Schematic illustration of exciton-exciton annihilation processes in monolayer WSe_2. (a) The annihilation of two A excitons (purple) gives rise to a higher-lying HX exciton (green). (b) We distinguish between three different Auger scattering processes: intravalley processes (I, blue) between KK excitons resulting in a final higher-lying KK exciton state, intervalley processes involving scattering between KΛ (II, yellow) or KK' (III, orange) excitons where the final state is a KΓ exciton. Figure is taken from Ref. [108] (Paper II).

[1]Intriguingly, the higher-lying conduction bands which make the scattering processes most resonant are negatively curved. This puts a constraint on the reduced exciton mass to be positive and for the final exciton state to be bound such that $|m_e| > |m_h|$. Luckily, this condition holds for our final states, and the existence of higher-lying exciton states has recently been established in monolayer and bilayer WSe_2 experimentally through up-converted photoluminescence measurements [105, 106].

5.1 Excitonic Auger Hamiltonian

Quantitatively, we address exciton-exciton annihilation in TMD monolayers by starting off from a purely electronic Hamiltonian:

$$H_{\mathrm{Aug}} = \sum_{\mathbf{k}_1,\mathbf{k}_2,\mathbf{q},\xi_1,\xi_2,\xi_3,\xi_4} W_{el,\mathbf{q}}^{\xi_1\xi_2\xi_3\xi_4} c'^{\dagger}_{\xi_1,\mathbf{k}_1+\mathbf{q}} v^{\dagger}_{\xi_2,\mathbf{k}_2-\mathbf{q}} c_{\xi_3,\mathbf{k}_2} c_{\xi_4,\mathbf{k}_1} + \mathrm{h.c.} \tag{5.1}$$

Here, $W_{el,\mathbf{q}}^{\xi_1..\xi_4}$ is the electronic Auger matrix element determining the probability of scattering between different conduction bands $c^{(\prime)}$ and valence bands v in valleys $\xi_1...\xi_4$ with a momentum transfer $\mathbf{q}$. In this matrix element, the screened interband Coulomb interaction (2.9) crucially enters, which in particular depends on the optical matrix element, M, determining the transition probability of scattering between conduction and valence bands. As the optical matrix element depends strongly on electronic wave function overlaps, it has been extracted from ab-initio calculations, performed by Roland Gillen, Friedrich-Alexander Universität, Erlangen-Nuremberg.

We will now proceed to find the excitonic analogue of (5.1). In this work, this is done by performing the three following steps (by perfect analogy with the procedure of finding the mean-field exciton-exciton Hamiltonian in Section 3.4): **i)** compute the equation of motion for the microscopic polarisation using (5.1), **ii)** transform the resulting equation to the exciton basis and **iii)** assume an excitonic Hamiltonian of the form $H_{x,\mathrm{Aug}} = \sum_{\mu,\nu,\rho,\mathbf{Q},\mathbf{Q}'} W_{\mathbf{Q},\mathbf{Q}'}^{\mu\nu\rho} Y^{\dagger}_{\mu,\mathbf{Q}+\mathbf{Q}'} X_{\nu,\mathbf{Q}} X_{\rho,\mathbf{Q}'}$, where $Y^{\dagger}$ creates a higher-lying exciton composed by an electron from the higher-lying conduction band c' and valence band v and X annihilates two conventional A excitons, cf. Fig. 5.1(a). The *excitonic* Auger matrix element $W_{\mathbf{Q},\mathbf{Q}'}^{\mu\nu\rho}$ is then obtained by demanding bosonic commutator relations for the exciton operators, deriving the corresponding equation of motion directly in the exciton picture and comparing the result with the equation from step **ii)**. Having laid out the procedure in great detail in the Supplementary Material of Paper II, we will here just note that the resulting excitonic Auger matrix element, besides being directly dependent on the electronic Auger interaction, also depends on the excitonic wave function overlaps between HX and A excitons. In summary, we find the following excitonic Hamiltonian describing exciton-exciton annihilation

$$H_{x,\mathrm{Aug}} = \frac{1}{2} \sum_{\mu,\nu,\rho,\mathbf{Q},\mathbf{Q}'} W_{\mathbf{Q},\mathbf{Q}'}^{\mu\nu\rho} Y^{\dagger}_{\mu,\mathbf{Q}+\mathbf{Q}'} X_{\nu,\mathbf{Q}} X_{\rho,\mathbf{Q}'} + \mathrm{h.c.}\ . \tag{5.2}$$

Here, we fix the initial exciton states to be $\nu = \rho = 1s$ as these states will be mostly occupied, but allow the final exciton state to be $\mu = 1s,2s,3s$. As shown in Paper II, the excitonic Auger matrix element decays rapidly with final exciton state due to the shrinking overlap with the initial 1s states, so it suffices to take into account $\mu < 3s$ in our calculations.

5.2 Temperature-dependent Auger recombination rates

Exciton-exciton annihilation can be experimentally addressed by means of time-resolved photoluminescence measurements and through the exciton-exciton annihilation rate or Auger coefficient, in the following denoted R_A. In particular, EEA is seen to lead to an effective saturation of exciton densities at high pump powers, and is limiting the efficiency of technologically relevant devices such as lasers or LEDs [109]. Here, we get microscopic access to the Auger coefficient by considering the Heisenberg equation of motion for the initial A exciton density $n_x = \sum_{\nu\mathbf{Q}} N^{\nu}_{\mathbf{Q}}$ reading $\dot{n}_x = -R_A n_x^2$ which upon applying the second order Born-Markov approximation[2] reads

$$R_A = \frac{2\pi}{\hbar} \sum_{\mu\nu\rho,\mathbf{Q},\mathbf{Q}'} |W^{\mu\nu\rho}_{\mathbf{Q},\mathbf{Q}'}|^2 N^{\nu}_{A,\mathbf{Q}} N^{\rho}_{A,\mathbf{Q}'} \delta(\Delta\epsilon) \ , \tag{5.3}$$

where $\Delta\epsilon$ expresses energy conservation between initial (A) and final (HX) exciton states in the scattering process and includes differences in HX and A exciton center-of-mass dispersions (cf. Eq. (2.30)) and single particle energy separations. As we estimate the appearing A exciton occupations $N^{\nu}_{A,\mathbf{Q}}$ with Boltzmann distributions, the Auger coefficient becomes explicitly temperature-dependent.

We have numerically evaluated the Auger coefficient for the exemplary hBN-encapsulated WSe_2 monolayer, revealing a highly non-monotonous dependence with respect to temperature as shown in Fig. 5.2(a). This temperature

[2]This approximation is commonly used when treating scattering processes. By applying the second order Born approximation we keep only terms which are quadratic in the exciton occupation (and neglect higher-order correlations) and within the Markov approximation non-linearities caused by quantum memory effects are neglected so that adiabatic solutions which express energy-conserving scattering processes can be obtained [85].

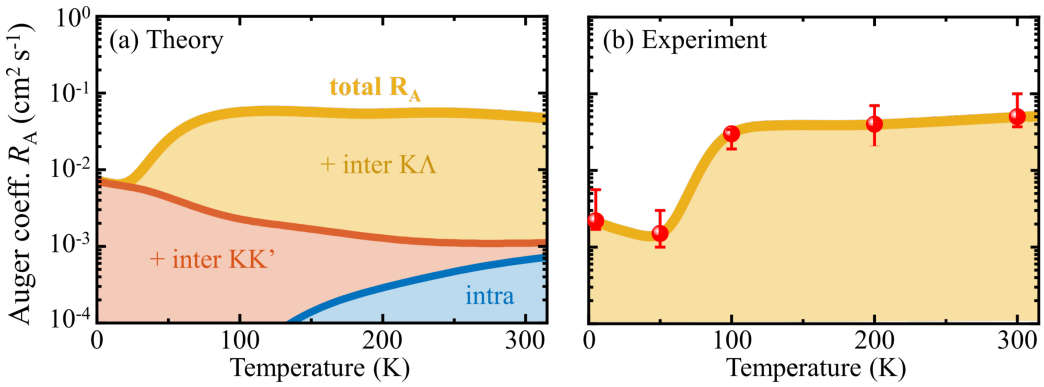

Figure 5.2: Temperature-dependent Auger coefficients in hBN-encapsulated monolayer WSe_2. (a) Calculated Auger coefficient separating contributions from intra- and intervalley processes, revealing the crucial importance of intervalley KΛ-KΛ scattering channels at room temperature. (b) Temperature-dependent Auger coefficients as extracted from time-resolved photoluminescence measurements. Figure adapted from Ref. [108] (Paper II).

dependence is explained through the interplay of KK', KΛ and KK A exciton occupations at different temperatures and reflects well the temperature dependence of valley-specific densities, $n_x^\nu(T) = \sum_{\boldsymbol{Q}} N_{A,\boldsymbol{Q}}^\nu(T)$, as obtained by the Boltzmann distribution. In Fig. 5.2(a) we have separated contributions stemming from intravalley Auger processes (process I in Fig. 5.1 (b)) and intervalley Auger recombination (processes II and III in Fig. 5.1 (b)). Crucially, we find that the impact of intravalley processes on the EEA is negligible, reflecting the low occupation of KK excitons at all temperatures. In contrast, the *dark* intervalley KΛ scattering channel is highly efficient. This is due to two reasons: **i**) a predominant occupation of KΛ excitons at room temperature, being a consequence of the three-fold degeneracy of the Λ valley and energetic ordering of bright and dark exciton states in WSe_2 (Fig. 2.1(b)) [31], **ii)** optimal energy separations and resonance conditions for the scattering to occur (given by $\Delta\epsilon$ in (5.3)). Note that the size of the excitonic Auger matrix element of the KΛ channel relative to the KK channel intriguingly plays a minor role for the scattering efficiency, despite the large momentum transfer entering and suppressing the KΛ matrix element.

In Fig. 5.2 (b) we present the Auger coefficients as extracted from time- and temperature-resolved photoluminescence measurements conducted by

the group of Alexey Chernikov (TU Dresden/University of Regensburg). We find an excellent agreement between theory and experiment - clearly revealing the impact of dark Auger recombination processes in the exciton-exciton annihilation in WSe_2. Hence, intriguingly, this study shows that dark excitons, although not being directly accessible by light, can contribute to the efficiency of exciton-based devices as efficient Auger recombination rates are seen to fundamentally lead to a saturation of exciton densities. Overall, our work provides experimentally and technologically viable pathways to tune and design inelastic many-body interactions in nanostructured systems.

CHAPTER 6

CONCLUSION AND OUTLOOK

6.1 Concluding remarks

In this thesis, we have unveiled the fundamental interaction mechanisms between different types of excitons in transition-metal dichalcogenide monolayers and van der Waals heterostructures. By making use of a fully quantum-mechanical microscopic approach relying on the exciton density matrix formalism we have addressed the importance of exciton-exciton interactions at elevated electron-hole pair densities in exciton dynamics, optics and transport. Our work is of fundamental as well as technological relevance. We have developed a microscopic theory for interactions between intra- and interlayer excitons and displayed their completely separate natures: intralayer excitons exhibit strong exchange interactions stemming from their fermionic substructure and interlayer excitons can be seen as repelling dipoles due to the spatial separation of their constituents. Moreover, we have shed light on the role of exciton-exciton interactions in Auger recombination processes known to limit the performance of photodetectors and solar cells, and exciton transport, which is crucial to be able to control when designing exciton-based transistors or other devices.

6.2 Outlook

Despite the fact that the first transition-metal dichalcogenide monolayer was successfully exfoliated only a decade ago, the field of two-dimensional materials is today dominated by the study of more complex structures including van der Waals heterostructures or moiré materials. In this thesis, we have devoted some attention to heterobilayers, but moiré structures are left for future studies. These novel and exotic structures, which may be formed by stacking two TMD layers with a relative twist angle with respect to each other (cf. Fig. 6.1), are seen to exhibit extremely intriguing many-body phenomena such as strongly correlated states and non-trivial topology induced by flat electronic bands. Moreover, as the electronic band structure is crucially affected by twisting, the excitonic landscape of the heterostructure changes and intra- and interlayer exciton states become strongly hybridised. Hybrid excitons, being a combination of intra- and interlayer excitons, also appear in untwisted structures, and typically in heterostructures with a dark ground state not covered in thesis. This opens up new horizons for future studies on exciton-exciton interactions: by tuning the intra- versus interlayer content of hybrid excitons also the nature of the interexcitonic interactions could be altered, providing new ways to manipulate optical properties and exciton transport.

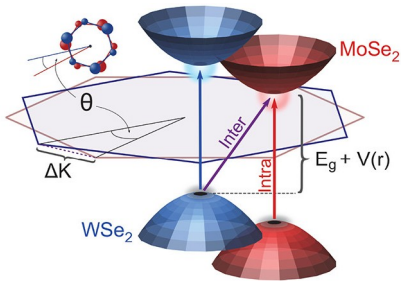

Figure 6.1: Schematic illustration of moiré excitons in the exemplary $MoSe_2$-WSe_2 heterostructure. By twisting the Mo- and W-layers with respect to each other, a moiré pattern is formed giving rise to a spatially dependent moiré potential, $V(r)$. Figure has been adapted from [70].

BIBLIOGRAPHY

[1] KS Novoselov. Nobel lecture: Graphene: Materials in the flatland. *Reviews of Modern Physics*, 83(3):837, 2011.

[2] Kin Fai Mak, Changgu Lee, James Hone, Jie Shan, and Tony F. Heinz. Atomically thin MoS_2: A new direct-gap semiconductor. *Physical Review Letters*, 105:136805, 2010.

[3] Zefang Wang, Daniel A Rhodes, Kenji Watanabe, Takashi Taniguchi, James C Hone, Jie Shan, and Kin Fai Mak. Evidence of high-temperature exciton condensation in two-dimensional atomic double layers. *Nature*, 574(7776):76–80, 2019.

[4] Anshul Kogar, Melinda S Rak, Sean Vig, Ali A Husain, Felix Flicker, Young Il Joe, Luc Venema, Greg J MacDougall, Tai C Chiang, Eduardo Fradkin, et al. Signatures of exciton condensation in a transition metal dichalcogenide. *Science*, 358(6368):1314–1317, 2017.

[5] Eva Y Andrei, Dmitri K Efetov, Pablo Jarillo-Herrero, Allan H MacDonald, Kin Fai Mak, T Senthil, Emanuel Tutuc, Ali Yazdani, and Andrea F Young. The marvels of moiré materials. *Nature Reviews Materials*, 6(3):201–206, 2021.

[6] Samuel Brem and Ermin Malic. Terahertz fingerprint of monolayer Wigner crystals. *Nano Letters*, 2022.

[7] Michele Cotrufo, Liuyang Sun, Junho Choi, Andrea Alù, and Xiaoqin Li. Enhancing functionalities of atomically thin semiconductors with plasmonic nanostructures. *Nanophotonics*, 8(4):577–598, 2019.

[8] Thomas Mueller and Ermin Malic. Exciton physics and device application of two-dimensional transition metal dichalcogenide semiconductors. *npj 2D Materials and Applications*, 2(1):1–12, 2018.

[9] Dominik Christiansen, Malte Selig, Gunnar Berghäuser, Robert Schmidt, Iris Niehues, Robert Schneider, Ashish Arora, Steffen Michaelis de Vasconcellos, Rudolf Bratschitsch, Ermin Malic, et al. Phonon sidebands in monolayer transition metal dichalcogenides. *Physical Review Letters*, 119(18):187402, 2017.

[10] Samuel Brem, August Ekman, Dominik Christiansen, Florian Katsch, Malte Selig, Cedric Robert, Xavier Marie, Bernhard Urbaszek, Andreas Knorr, and Ermin Malic. Phonon-assisted photoluminescence from indirect excitons in monolayers of transition-metal dichalcogenides. *Nano Letters*, 20(4):2849–2856, 2020.

[11] Zhipeng Li, Tianmeng Wang, Chenhao Jin, Zhengguang Lu, Zhen Lian, Yuze Meng, Mark Blei, Shiyuan Gao, Takashi Taniguchi, Kenji Watanabe, et al. Emerging photoluminescence from the dark-exciton phonon replica in monolayer WSe_2. *Nature Communications*, 10(1):1–7, 2019.

[12] Samuel Brem, Jonas Zipfel, Malte Selig, Archana Raja, Lutz Waldecker, Jonas D Ziegler, Takashi Taniguchi, Kenji Watanabe, Alexey Chernikov, and Ermin Malic. Intrinsic lifetime of higher excitonic states in tungsten diselenide monolayers. *Nanoscale*, 11(25):12381–12387, 2019.

[13] Giovanna Panzarini, Lucio Claudio Andreani, A Armitage, D Baxter, MS Skolnick, VN Astratov, JS Roberts, Alexey V Kavokin, Maria R Vladimirova, and MA Kaliteevski. Exciton-light coupling in single and coupled semiconductor microcavities: Polariton dispersion and polarization splitting. *Physical Review B*, 59(7):5082, 1999.

[14] Jacek Kasprzak, Murielle Richard, S Kundermann, A Baas, P Jeambrun, Jonathan Mark James Keeling, FM Marchetti, MH Szymańska,

R André, JL Staehli, et al. Bose–Einstein condensation of exciton polaritons. *Nature*, 443(7110):409–414, 2006.

[15] Jamie M Fitzgerald, Joshua JP Thompson, and Ermin Malic. Twist angle tuning of moiré exciton polaritons in van der Waals heterostructures. *arXiv preprint arXiv:2201.08437*, 2022.

[16] H Wang, KB Ferrio, DG Steel, PR Berman, YZ Hu, R Binder, and SW Koch. Transient four-wave-mixing line shapes: effects of excitation-induced dephasing. *Physical Review A*, 49(3):R1551, 1994.

[17] Hans Christian Schneider, Weng Wah Chow, and Stephan W Koch. Excitation-induced dephasing in semiconductor quantum dots. *Physical Review B*, 70(23):235308, 2004.

[18] Nardeep Kumar, Qiannan Cui, Frank Ceballos, Dawei He, Yongsheng Wang, and Hui Zhao. Exciton-exciton annihilation in $MoSe_2$ monolayers. *Physical Review B*, 89(12):125427, 2014.

[19] A Suna. Kinematics of exciton-exciton annihilation in molecular crystals. *Physical Review B*, 1(4):1716, 1970.

[20] Miguel M Ugeda, Aaron J Bradley, Su-Fei Shi, H Felipe, Yi Zhang, Diana Y Qiu, Wei Ruan, Sung-Kwan Mo, Zahid Hussain, Zhi-Xun Shen, et al. Giant bandgap renormalization and excitonic effects in a monolayer transition metal dichalcogenide semiconductor. *Nature Materials*, 13(12):1091–1095, 2014.

[21] A Steinhoff, J-H Kim, F Jahnke, M Rosner, D-S Kim, Ch Lee, Gang Hee Han, Mun Seok Jeong, TO Wehling, and C Gies. Efficient excitonic photoluminescence in direct and indirect band gap monolayer MoS_2. *Nano Letters*, 15(10):6841–6847, 2015.

[22] D Erben, A Steinhoff, C Gies, G Schönhoff, TO Wehling, and F Jahnke. Excitation-induced transition to indirect band gaps in atomically thin transition-metal dichalcogenide semiconductors. *Physical Review B*, 98(3):035434, 2018.

[23] Jonas Zipfel, Marvin Kulig, Raül Perea-Causín, Samuel Brem, Jonas D Ziegler, Roberto Rosati, Takashi Taniguchi, Kenji Watanabe,

Mikhail M Glazov, Ermin Malic, et al. Exciton diffusion in monolayer semiconductors with suppressed disorder. *Physical Review B*, 101(11):115430, 2020.

[24] Darwin F Cordovilla Leon, Zidong Li, Sung Woon Jang, and Parag B Deotare. Hot exciton transport in WSe_2 monolayers. *Physical Review B*, 100(24):241401, 2019.

[25] Long Yuan, Biyuan Zheng, Jens Kunstmann, Thomas Brumme, Agnieszka Beata Kuc, Chao Ma, Shibin Deng, Daria Blach, Anlian Pan, and Libai Huang. Twist-angle-dependent interlayer exciton diffusion in $WS_2 - WSe_2$ heterobilayers. *Nature Materials*, 19(6):617–623, 2020.

[26] C Ciuti, V Savona, C Piermarocchi, A Quattropani, and P Schwendimann. Role of the exchange of carriers in elastic exciton-exciton scattering in quantum wells. *Physical Review B*, 58(12):7926, 1998.

[27] Robert Wallauer, Raul Perea-Causin, Lasse Munster, Sarah Zajusch, Samuel Brem, Jens Gudde, Katsumi Tanimura, Kai-Qiang Lin, Rupert Huber, Ermin Malic, et al. Momentum-resolved observation of exciton formation dynamics in monolayer WS_2. *Nano Letters*, 21(13):5867–5873, 2021.

[28] Malte Selig, Gunnar Berghäuser, Marten Richter, Rudolf Bratschitsch, Andreas Knorr, and Ermin Malic. Dark and bright exciton formation, thermalization, and photoluminescence in monolayer transition metal dichalcogenides. *2D Materials*, 5(3):035017, 2018.

[29] Gunnar Berghäuser, Philipp Steinleitner, Philipp Merkl, Rupert Huber, Andreas Knorr, and Ermin Malic. Mapping of the dark exciton landscape in transition metal dichalcogenides. *Physical Review B*, 98(2):020301, 2018.

[30] Hongyi Yu, Gui-Bin Liu, Pu Gong, Xiaodong Xu, and Wang Yao. Dirac cones and Dirac saddle points of bright excitons in monolayer transition metal dichalcogenides. *Nature Communications*, 5(1):1–7, 2014.

[31] Ermin Malic, Malte Selig, Maja Feierabend, Samuel Brem, Dominik Christiansen, Florian Wendler, Andreas Knorr, and Gunnar Berghäuser. Dark excitons in transition metal dichalcogenides. *Physical Review Materials*, 2(1):014002, 2018.

[32] Julien Madéo, Michael KL Man, Chakradhar Sahoo, Marshall Campbell, Vivek Pareek, E Laine Wong, Abdullah Al-Mahboob, Nicholas S Chan, Arka Karmakar, Bala Murali Krishna Mariserla, et al. Directly visualizing the momentum-forbidden dark excitons and their dynamics in atomically thin semiconductors. *Science*, 370(6521):1199–1204, 2020.

[33] Yuan Liu, Nathan O Weiss, Xidong Duan, Hung-Chieh Cheng, Yu Huang, and Xiangfeng Duan. Van der Waals heterostructures and devices. *Nature Reviews Materials*, 1(9):1–17, 2016.

[34] Pasqual Rivera, John R Schaibley, Aaron M Jones, Jason S Ross, Sanfeng Wu, Grant Aivazian, Philip Klement, Kyle Seyler, Genevieve Clark, Nirmal J Ghimire, et al. Observation of long-lived interlayer excitons in monolayer $MoSe_2$-WSe_2 heterostructures. *Nature Communications*, 6(1):1–6, 2015.

[35] Simon Ovesen, Samuel Brem, Christopher Linderälv, Mikael Kuisma, Tobias Korn, Paul Erhart, Malte Selig, and Ermin Malic. Interlayer exciton dynamics in van der Waals heterostructures. *Communications Physics*, 2(1):1–8, 2019.

[36] Zhe Sun, Alberto Ciarrocchi, Fedele Tagarelli, Juan Francisco Gonzalez Marin, Kenji Watanabe, Takashi Taniguchi, and Andras Kis. Excitonic transport driven by repulsive dipolar interaction in a van der Waals heterostructure. *Nature Photonics*, 16:79–85, 2021.

[37] Qingjun Tong, Hongyi Yu, Qizhong Zhu, Yong Wang, Xiaodong Xu, and Wang Yao. Topological mosaics in moiré superlattices of van der Waals heterobilayers. *Nature Physics*, 13(4):356–362, 2017.

[38] Yuan Cao, Valla Fatemi, Shiang Fang, Kenji Watanabe, Takashi Taniguchi, Efthimios Kaxiras, and Pablo Jarillo-Herrero. Unconventional superconductivity in magic-angle graphene superlattices. *Nature*, 556(7699):43–50, 2018.

[39] Michael Peskin. *An Introduction to Quantum Field Theory*. CRC press, 2018.

[40] Gerald D Mahan. *Many-particle Physics*. Springer Science & Business Media, 2013.

[41] Chetan Nayak, Steven H Simon, Ady Stern, Michael Freedman, and Sankar Das Sarma. Non-abelian anyons and topological quantum computation. *Reviews of Modern Physics*, 80(3):1083, 2008.

[42] Florian Katsch, Malte Selig, Alexander Carmele, and Andreas Knorr. Theory of exciton–exciton interactions in monolayer transition metal dichalcogenides. *physica status solidi (b)*, 255(12):1800185, 2018.

[43] AL Ivanov and H Haug. Self-consistent theory of the biexciton optical nonlinearity. *Physical Review B*, 48(3):1490, 1993.

[44] Tunemaru Usui. Excitations in a high density electron gas. i. *Progress of Theoretical Physics*, 23(5):787–798, 1960.

[45] Gunnar Berghäuser and Ermin Malic. Analytical approach to excitonic properties of MoS_2. *Physical Review B*, 89(12):125309, 2014.

[46] Hartmut Haug and Stephan W Koch. *Quantum theory of the optical and electronic properties of semiconductors*. World Scientific Publishing Company, 2009.

[47] Natalia S Rytova. Screened potential of a point charge in a thin film. *Moscow University Physics Bulletin*, 3(30), 1967.

[48] LV Keldysh. Coulomb interaction in thin semiconductor and semimetal films. *Soviet Journal of Experimental and Theoretical Physics Letters*, 29:658, 1979.

[49] Pierluigi Cudazzo, Ilya V Tokatly, and Angel Rubio. Dielectric screening in two-dimensional insulators: Implications for excitonic and impurity states in graphane. *Physical Review B*, 84(8):085406, 2011.

[50] Mads L Trolle, Thomas G Pedersen, and Valerie Véniard. Model dielectric function for 2d semiconductors including substrate screening. *Scientific Reports*, 7(1):1–9, 2017.

[51] Gunnar Berghäuser and Ermin Malic. Analytical approach to excitonic properties of MoS_2. *Physical Review B*, 89:125309, Mar 2014.

[52] Ermin Malic, Malte Selig, Maja Feierabend, Samuel Brem, Dominik Christiansen, Florian Wendler, Andreas Knorr, and Gunnar

Berghäuser. Dark excitons in transition metal dichalcogenides. *Physical Review Materials*, 2:014002, Jan 2018.

[53] Torben Winzer, Andreas Knorr, and Ermin Malic. Carrier multiplication in graphene. *Nano Letters*, 10(12):4839–4843, 2010.

[54] Feng Wang, Yang Wu, Mark S Hybertsen, and Tony F Heinz. Auger recombination of excitons in one-dimensional systems. *Physical Review B*, 73(24):245424, 2006.

[55] Philipp Merkl, Fabian Mooshammer, Philipp Steinleitner, Anna Girnghuber, K-Q Lin, Philipp Nagler, Johannes Holler, Christian Schüller, John M Lupton, Tobias Korn, et al. Ultrafast transition between exciton phases in van der Waals heterostructures. *Nature Materials*, 18(7):691–696, 2019.

[56] Akash Laturia, Maarten L Van de Put, and William G Vandenberghe. Dielectric properties of hexagonal boron nitride and transition metal dichalcogenides: from monolayer to bulk. *npj 2D Materials and Applications*, 2(1):1–7, 2018.

[57] R Geick, CH Perry, and GJPR Rupprecht. Normal modes in hexagonal boron nitride. *Physical Review*, 146(2):543, 1966.

[58] Simone Latini, Thomas Olsen, and Kristian Sommer Thygesen. Excitons in van der Waals heterostructures: The important role of dielectric screening. *Physical Review B*, 92(24):245123, 2015.

[59] Diana Y Qiu, H Felipe, and Steven G Louie. Screening and many-body effects in two-dimensional crystals: Monolayer MoS_2. *Physical Review B*, 93(23):235435, 2016.

[60] M Kira and SW Koch. Many-body correlations and excitonic effects in semiconductor spectroscopy. *Progress in Quantum Electronics*, 30(5):155–296, 2006.

[61] LJ Sham and TM Rice. Many-particle derivation of the effective-mass equation for the Wannier exciton. *Physical Review*, 144(2):708, 1966.

[62] Jacov Frenkel. On the transformation of light into heat in solids. i. *Physical Review*, 37(1):17, 1931.

[63] Roman Schuster, Martin Knupfer, and Helmuth Berger. Exciton band structure of pentacene molecular solids: breakdown of the frenkel exciton model. *Physical Review Letters*, 98(3):037402, 2007.

[64] Samuel Brem, Malte Selig, Gunnar Berghaeuser, and Ermin Malic. Exciton relaxation cascade in two-dimensional transition metal dichalcogenides. *Scientific Reports*, 8(1):1–8, 2018.

[65] Maja Feierabend, Gunnar Berghäuser, Andreas Knorr, and Ermin Malic. Proposal for dark exciton based chemical sensors. *Nature Communications*, 8(1):1–6, 2017.

[66] Toshio Marumori, Masatoshi Yamamura, and Akira Tokunaga. On the "anharmonic effects" on the collective oscillations in spherical even nuclei. i. *Progress of Theoretical Physics*, 31(6):1009–1025, 1964.

[67] Eiichi Hanamura. Theory of the high density exciton. i. *Journal of the Physical Society of Japan*, 29(1):50–57, 1970.

[68] Philipp Merkl, Fabian Mooshammer, Samuel Brem, Anna Girnghuber, Kai-Qiang Lin, Leonard Weigl, Marlene Liebich, Chaw-Keong Yong, Roland Gillen, Janina Maultzsch, et al. Twist-tailoring Coulomb correlations in van der Waals homobilayers. *Nature Communications*, 11(1):1–7, 2020.

[69] Samuel Brem, Kai-Qiang Lin, Roland Gillen, Jonas M Bauer, Janina Maultzsch, John M Lupton, and Ermin Malic. Hybridized intervalley moiré excitons and flat bands in twisted WSe_2 bilayers. *Nanoscale*, 12(20):11088–11094, 2020.

[70] Samuel Brem, Christopher Linderälv, Paul Erhart, and Ermin Malic. Tunable phases of moiré excitons in van der Waals heterostructures. *Nano Letters*, 20(12):8534–8540, 2020.

[71] Junho Choi, Wei-Ting Hsu, Li-Syuan Lu, Liuyang Sun, Hui-Yu Cheng, Ming-Hao Lee, Jiamin Quan, Kha Tran, Chun-Yuan Wang, Matthew Staab, et al. Moiré potential impedes interlayer exciton diffusion in van der Waals heterostructures. *Science advances*, 6(39):eaba8866, 2020.

[72] Galan Moody, Chandriker Kavir Dass, Kai Hao, Chang-Hsiao Chen, Lain-Jong Li, Akshay Singh, Kha Tran, Genevieve Clark, Xiaodong

Xu, Gunnar Berghäuser, et al. Intrinsic homogeneous linewidth and broadening mechanisms of excitons in monolayer transition metal dichalcogenides. *Nature Communications*, 6(1):1–6, 2015.

[73] Philipp Nagler, Gerd Plechinger, Mariana V Ballottin, Anatolie Mitioglu, Sebastian Meier, Nicola Paradiso, Christoph Strunk, Alexey Chernikov, Peter CM Christianen, Christian Schüller, et al. Interlayer exciton dynamics in a dichalcogenide monolayer heterostructure. *2D Materials*, 4(2):025112, 2017.

[74] M. Combescot, O. Betbeder-Matibet, and R. Combescot. Exciton-exciton scattering: Composite boson versus elementary boson. *Physical Review B*, 75:174305, 2007.

[75] Christoph Schindler and Roland Zimmermann. Analysis of the exciton-exciton interaction in semiconductor quantum wells. *Physical Review B*, 78(4):045313, 2008.

[76] Daniel Erkensten, Samuel Brem, and Ermin Malic. Exciton-exciton interaction in transition metal dichalcogenide monolayers and van der Waals heterostructures. *Physical Review B*, 103:045426, Jan 2021.

[77] Andre K Geim and Irina V Grigorieva. Van der Waals heterostructures. *Nature*, 499(7459):419–425, 2013.

[78] Roland Gillen and Janina Maultzsch. Interlayer excitons in $MoSe_2/WSe_2$ heterostructures from first principles. *Physical Review B*, 97(16):165306, 2018.

[79] Samuel Brem. *Microscopic Theory of Exciton Dynamics in Two-Dimensional Materials*. PhD thesis, Chalmers University of Technology, 2021.

[80] Zhenghe Jin, Xiaodong Li, Jeffrey T. Mullen, and Ki Wook Kim. Intrinsic transport properties of electrons and holes in monolayer transition-metal dichalcogenides. *Physical Review B*, 90:045422, 2014.

[81] Joshua JP Thompson, Samuel Brem, Hanlin Fang, Carlos Antón-Solanas, Bo Han, Hangyong Shan, Saroj P Dash, Witlef Wieczorek, Christian Schneider, and Ermin Malic. Valley-exchange coupling

probed by angle-resolved photoluminescence. *Nanoscale Horizons*, 7(1):77–84, 2022.

[82] Joshua Thompson, Samuel Brem, Marne Verjans, Ermin Malic, Rudolf Bratschitsch, Steffen Michaelis de Vasconcellos, and Robert Schmidt. Anisotropic exciton diffusion in atomically-thin semiconductors. *2D Materials*, 2022.

[83] F. Tassone and Y. Yamamoto. Exciton-exciton scattering dynamics in a semiconductor microcavity and stimulated scattering into polaritons. *Physical Review B*, 59:10830–10842, 1999.

[84] AI Bobrysheva, MF Miglei, and MI Shmiglyuk. On the bi-exciton formation in crystals. *physica status solidi (b)*, 53(1):71–84, 1972.

[85] Mackillo Kira and Stephan W. Koch. *Semiconductor Quantum Optics*. Cambridge University Press, 2011.

[86] G Röpke and R Der. The influence of two-particle states (excitons) on the dielectric function of the electron—hole plasma. *physica status solidi (b)*, 92(2):501–510, 1979.

[87] Niels Bohr and Jens Lindhard. *Electron capture and loss by heavy ions penetrating through matter*, volume 28. Dan. Mat. Fys, 1954.

[88] J. Fernández-Rossier, C. Tejedor, L. Muñoz, and L. Viña. Polarized interacting exciton gas in quantum wells and bulk semiconductors. *Physical Review B*, 54:11582–11591, 1996.

[89] V. Shahnazaryan, I. Iorsh, I. A. Shelykh, and O. Kyriienko. Exciton-exciton interaction in transition-metal dichalcogenide monolayers. *Physical Review B*, 96:115409, 2017.

[90] Tomasz Woźniak, Paulo E. Faria Junior, Gotthard Seifert, Andrey Chaves, and Jens Kunstmann. Exciton g factors of van der Waals heterostructures from first-principles calculations. *Physical Review B*, 101:235408, 2020.

[91] Lars Hedin. New method for calculating the one-particle green's function with application to the electron-gas problem. *Physical Review*, 139:A796–A823, 1965.

[92] Joakim Hagel, Samuel Brem, Christopher Linderälv, Paul Erhart, and Ermin Malic. Exciton landscape in van der Waals heterostructures. *Physical Review Research*, 3(4):043217, 2021.

[93] D. Erben, A. Steinhoff, C. Gies, G. Schönhoff, T. O. Wehling, and F. Jahnke. Excitation-induced transition to indirect band gaps in atomically thin transition-metal dichalcogenide semiconductors. *Physical Review B*, 98:035434, 2018.

[94] Koloman Wagner, Jonas Zipfel, Roberto Rosati, Edith Wietek, Jonas D. Ziegler, Samuel Brem, Raül Perea-Causín, Takashi Taniguchi, Kenji Watanabe, Mikhail M. Glazov, Ermin Malic, and Alexey Chernikov. Nonclassical exciton diffusion in monolayer WSe_2. *Physical Review Letters*, 127:076801, Aug 2021.

[95] Roberto Rosati, Raül Perea-Causín, Samuel Brem, and Ermin Malic. Negative effective excitonic diffusion in monolayer transition metal dichalcogenides. *Nanoscale*, 12(1):356–363, 2020.

[96] Roberto Rosati, Robert Schmidt, Samuel Brem, Raül Perea-Causín, Iris Niehues, Johannes Kern, Johann A Preuß, Robert Schneider, Steffen Michaelis de Vasconcellos, Rudolf Bratschitsch, et al. Dark exciton anti-funneling in atomically thin semiconductors. *Nature Communications*, 12(1):1–7, 2021.

[97] Ortwin Hess and Tilmann Kuhn. Maxwell-Bloch equations for spatially inhomogeneous semiconductor lasers. i. Theoretical formulation. *Physical Review A*, 54:3347–3359, 1996.

[98] Raul Perea-Causin, Samuel Brem, Roberto Rosati, Roland Jago, Marvin Kulig, Jonas D Ziegler, Jonas Zipfel, Alexey Chernikov, and Ermin Malic. Exciton propagation and halo formation in two-dimensional materials. *Nano Letters*, 19(10):7317–7323, 2019.

[99] AL Ivanov. Quantum diffusion of dipole-oriented indirect excitons in coupled quantum wells. *EPL (Europhysics Letters)*, 59(4):586, 2002.

[100] Jue Wang, Qianhui Shi, En-Min Shih, Lin Zhou, Wenjing Wu, Yusong Bai, Daniel Rhodes, Katayun Barmak, James Hone, Cory R.

Dean, and X.-Y. Zhu. Diffusivity reveals three distinct phases of interlayer excitons in $MoSe_2/WSe_2$ heterobilayers. *Physical Review Letters*, 126:106804, Mar 2021.

[101] Yuya Shimazaki, Ido Schwartz, Kenji Watanabe, Takashi Taniguchi, Martin Kroner, and Ataç Imamoğlu. Strongly correlated electrons and hybrid excitons in a moiré heterostructure. *Nature*, 580(7804):472–477, 2020.

[102] Yanhao Tang, Jie Gu, Song Liu, Kenji Watanabe, Takashi Taniguchi, James Hone, Kin Fai Mak, and Jie Shan. Tuning layer-hybridized moiré excitons by the quantum-confined Stark effect. *Nature Nanotechnology*, 16(1):52–57, 2021.

[103] Torben Winzer and Ermin Malić. Impact of auger processes on carrier dynamics in graphene. *Physical Review B*, 85(24):241404, 2012.

[104] Xiao-Xiao Zhang, Yumeng You, Shu Yang Frank Zhao, and Tony F Heinz. Experimental evidence for dark excitons in monolayer WSe_2. *Physical Review Letters*, 115(25):257403, 2015.

[105] Kai-Qiang Lin, Chin Shen Ong, Sebastian Bange, Paulo E Faria Junior, Bo Peng, Jonas D Ziegler, Jonas Zipfel, Christian Bäuml, Nicola Paradiso, Kenji Watanabe, et al. Narrow-band high-lying excitons with negative-mass electrons in monolayer WSe_2. *Nature Communications*, 12(1):1–8, 2021.

[106] Kai-Qiang Lin, Paulo E Faria Junior, Jonas M Bauer, Bo Peng, Bartomeu Monserrat, Martin Gmitra, Jaroslav Fabian, Sebastian Bange, and John M Lupton. Twist-angle engineering of excitonic quantum interference and optical nonlinearities in stacked 2d semiconductors. *Nature Communications*, 12(1):1–7, 2021.

[107] B. Han, C. Robert, E. Courtade, M. Manca, S. Shree, T. Amand, P. Renucci, T. Taniguchi, K. Watanabe, X. Marie, L. E. Golub, M. M. Glazov, and B. Urbaszek. Exciton states in monolayer $MoSe_2$ and $MoTe_2$ probed by upconversion spectroscopy. *Physical Review X*, 8:031073, 2018.

[108] Daniel Erkensten, Samuel Brem, Koloman Wagner, Roland Gillen, Raül Perea-Causín, Jonas D Ziegler, Takashi Taniguchi, Kenji Watanabe, Janina Maultzsch, Alexey Chernikov, et al. Dark exciton-exciton annihilation in monolayer WSe_2. *Physical Review B*, 104(24):L241406, 2021.

[109] Shibin Deng, Enzheng Shi, Long Yuan, Linrui Jin, Letian Dou, and Libai Huang. Long-range exciton transport and slow annihilation in two-dimensional hybrid perovskites. *Nature Communications*, 11(1):1–8, 2020.